



Provided by the author(s) and University of Galway in accordance with publisher policies. Please cite the published version when available.

Title	In vitro model development for pulsed-field ablation treatment of atrial fibrillation
Author(s)	Baena Montes, Jara Maria
Publication Date	2024-04-15
Publisher	NUI Galway
Item record	http://hdl.handle.net/10379/18145

Downloaded 2024-05-02T19:08:16Z

Some rights reserved. For more information, please see the item record link above.



IN VITRO MODEL DEVELOPMENT FOR PULSED-FIELD ABLATION TREATMENT OF ATRIAL FIBRILLATION



OLLSCOIL NA
GAILLIMHÉ
UNIVERSITY
OF GALWAY

Candidate name: Jara Maria Baena Montes

ID: 21254710

Degree: Research Masters in Physiology

Supervisor: Dr. Leo Quinlan

Date of submission: 12th April 2024

TABLE OF CONTENTS

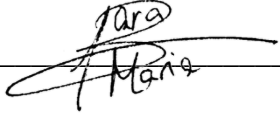
Introduction and Scopus of the Project	1
Chapter 1 – Literature Review	3
Introduction	3
Current experimental models of Atrial Fibrillation	9
In vivo models.....	9
Ex vivo models.....	12
In vitro models	14
Future perspectives and challenges in Atrial Fibrillation modelling	23
Chapter 2 – Electroporation Parameters for Human Cardiomyocyte Ablation	
In Vitro.....	24
Introduction	24
Materials & Methods	26
Results.....	29
Discussion	34
Conclusions	37
Chapter 3 – Optimization of a 3D Hydrogel Model for Cardiomyocyte	
Ablation In Vitro	38
Introduction	38
Materials and Methods	40
Results and Discussion	45
Conclusions	53
Chapter 4 – Conclusions.....	54

Declaration

This thesis is based on a group project with the team of Aurigen Medical, who provided the pulse generator and the 3D-printed probes used in Chapter 2 and 3.

Individual contributions are listed below:

- Dr Eoghan Dunne is a Research Fellow Translational Medical Device Lab (TMDLab), Lambe Institute of Translational Research in Galway, Ireland. He contributed to this work with the numerical modelling section in Chapter 2.
- Hamza Benchakroun is a PhD student in the Translational Medical Device Lab (TMDLab), Lambe Institute of Translational Research in Galway, Ireland. He contributed to this work with the conductivity measurements of the hydrogels in Chapter 3.

Signature:  _____

Date: 04/04/2023

Acknowledgments

I would like to express my gratitude to my primary supervisor, Dr Leo Quinlan, who guided me so positively and who always made me feel confident in my abilities. I would like to extend my sincere thanks to the team in Aurigen medical, for giving me the opportunity to work together with them and continuously learn from their expertise. I am also very grateful to my lab team, for their help, inspiration, and moral support in every step of this process. Lastly, I would be remiss in not mentioning my family, especially my mom. Her belief in me has kept my spirits and motivation high during this journey.

Abstract

Atrial fibrillation is the most common type of cardiac arrhythmias in humans, mostly based on hyperexcitation of specific areas in the atrium that results in dyssynchronous atrial contraction, leading to severe consequences such as heart failure and stroke. Among the current treatment options, catheter-based ablation is used to isolate and destroy the abnormal tissue in the heart that promotes atrial fibrillation and has shown to be a good alternative to anti-arrhythmic pharmacological treatment. However, due to the large number of parameters involved, the selection and optimization of a good in vitro model is essential before translating the treatment to clinical trials. To this aim, this project focuses on the development of three in vitro culture models to be used as ablation testing platforms and the information that they can provide, indicating their potential as models in different stages of the treatment testing. The models presented are connected so that the results of the simpler model will influence the parameter decision of more complex models, reducing the parameter range while increasing the physiological resemblance to the real cardiac tissue. This study concludes by highlighting the potential of irreversible electroporation as a treatment for atrial fibrillation and the valuable information that can be obtained from these models.

Introduction and Scope of the Project

Atrial fibrillation (Afib) is the most common type of arrhythmia, and its incidence increased significantly in the last century. The complexity of the Afib mechanisms and its intimate relationship with other heart diseases, makes it a challenging disease to treat correctly. Afib therapy development is an evolving field that aims to target this condition through different pharmacological and non-pharmacological approaches. In order to test and validate any of these treatments, an appropriate preclinical model must be carefully chosen to refine and optimise the therapy features to correctly reverse Afib.

Due to the importance of selecting a good model, this project focuses on the design of an appropriate in vitro model of Afib to optimise the parameter selection of pulsed field ablation treatment. To this aim, three in vitro models are developed and treated with selected ablation parameters, following the acquisition of different outputs (fluorescent reading, microscope imaging) and the analysis of these results to discuss the value of each model in ablation preclinical testing. Chapter 1 provides a detailed review of the current Afib models, together with their uses, advantages and limitations. After analysing the current in vitro options, two simple in vitro models were explored in Chapter 2, analysing effect of individual parameters such as the voltage or pulse width on cell death using suspension or monolayer models. 2D ablation imaging shows a useful way of detecting the ablation area distribution in early studies of in vitro ablation testing. Once this range of parameters was tested, a more complex model was designed in Chapter 3. This chapter goes through the optimization process of two candidate hydrogels, analysing their effect on cell viability, morphology and ultimately their potential as ablation models. This project concludes the usefulness of three different in vitro models of increasing complexity (cell suspension, cell monolayer and hydrogel) for preclinical testing of ablation treatments, highlighting the importance of choosing a good model not only for cell viability but also that can resist the physical properties of applying electrical pulses. This project was made in collaboration with other scientists that offered their knowledge and results regarding computational modelling (Chapter 2) and hydrogel conductivity measurements (Chapter 3) as indicated in the Declaration.

Chapter 1 – Literature Review

1. Introduction

Atrial fibrillation is the most common type of cardiac arrhythmias in humans, characterised by high-frequency excitation of the atrium that results in dyssynchronous atrial contraction and irregularities in ventricular excitation (1). The prevalence of Afib is increasing with an estimated 33 million people worldwide diagnosed with AFib in 2020 and this figure is expected to double by 2050 (2). AFib patients have increased morbidity and mortality rates as a result of severe consequences associated with thromboembolism and stroke (3). Moreover, COVID-19 infection is reported to be associated with more frequent occurrences of arrhythmias, predominantly AFib cases (4), making it a global concern that needs more efficient and effective treatment options.

Clinically AFib is divided into paroxysmal, persistent, long-standing persistent, or permanent, depending on the duration of the symptoms. Paroxysmal AFib resolves typically within 7 days of onset while persistent AFib is sustained for longer than 7 days. Long-standing persistent AFib lasts more than 12 months and AFib is considered permanent when there has been a joint decision by the patient and clinician to cease further attempts to restore or maintain sinus rhythm (5). The pathophysiology underlying Afib involves a complex process that is not yet fully understood. A key component in the maintenance of the AFib arrhythmia state is the process of re-entry, which occurs when an impulse travels abnormally around a cardiac circuit repetitively. This is a triggered process that initiates an arrhythmia, which is commonly induced by an ectopic firing focus. The first reported focal ectopic firing loci were found in the pulmonary veins (PVs) in patients with paroxysmal AF; ablation of these ectopic foci was shown to reduce AFib burden, demonstrating a role for PVs in AFib genesis (6). Several subsequent studies have provided evidence for the role of PVs in AFib initiation (7–9). These processes are defined as the group of molecular, cellular and interstitial changes that can manifest as changes in size, mass, geometry and function of the heart after injury (10). Some of these changes include progressive atrial dilatation (11) or

changes in ion channel activity, (particularly Na^+ and K^+ currents) (12). Overall this results in a vulnerable tissue substrate that facilitates the process of re-entry that maintains AFib. Re-entry itself is a process that occurs when a propagating impulse fails to fade after normal activation of the heart and persists, resulting in continuous re-excitation of the heart even after the refractory period has ended (Figure 1.1). Thus, re-entry requires some type of stimulus, that triggers a vulnerable circuit (tissue substrate) where its depolarizing signal never encounters refractory tissue (13). This translates into the typical increase in heart rate of arrhythmic patients.

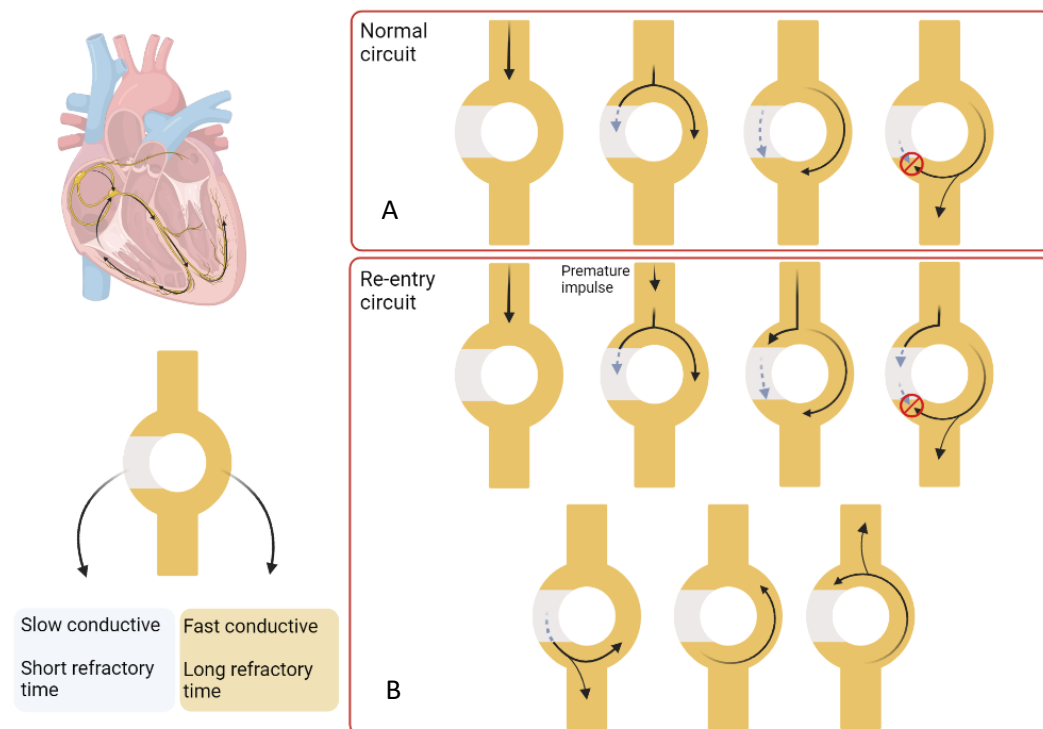


Figure 1.1. Process of re-entry in Afib. Most of the re-entry circuits happen above the level of the ventricles, but this process can take place in any area of the heart. This circuit consists of a single pathway that divides in two, one which shows slow conductivity and short refractory time and the other shows fast conductivity and longer refractory time. (A) In a normal circuit, an impulse travel through the circuit and splits in both pathways. The fast conductive pathway propagates the impulse quicker but the long refractory period makes it not accessible for a long time. The slow conductive pathway propagates the impulse slower, with a quicker recovery. When the impulse in the fast conductive pathway gets to the next pathway it splits again and propagates the impulse, while the other component will interact with the slow conductive pathway impulse and annulate each other. This way, the impulse is transmitted forward. (B) A re-entry circuit is promoted by a premature impulse, which would take the slow conductive pathway due to the short refractory time. This will lead to an impulse that does not fade and persists propagating impulses in both directions, leading to a continuous re-excitation of the heart. Created with BioRender.com.

Current therapeutic options

The main therapeutic goal in the management of AFib is the restoration and maintenance of a normal sinus rhythm. Anti-arrhythmic drugs (AADs) remain the most widely prescribed treatment for AFib patients; however, they are not always effective and show significant adverse effects, including that some are pro-arrhythmic (14). Anti-arrhythmic drugs typically act on ion channels with the main goal of reducing the frequency and duration of episodes of arrhythmias. AADs are classified depending on the mechanism of action and specific effects on the heart. Class I AADs are sodium channel blockers, and they reduce the conduction velocity and are commonly used to treat atrial and ventricular arrhythmias. They are further subdivided into IA (such as quinidine or procainamide), IB (such as lidocaine or mexiletine) and IC (such as flecainide and propafenone). Class II AADs are beta-blockers, and they by blocking epinephrine and norepinephrine from binding to the beta-adrenergic receptors, decreasing conduction through the AV node. Some examples are propranolol and metoprolol. Class III AADs block potassium channels, re-polarising the cells and prolonging the action potential duration. The most used are amiodarone, sotalol and dronedarone (15,16). However, the positive effect of these drugs on reducing mortality and other clinical factors remains unclear (14,15,17).

There is growing interest in non-pharmacological treatments as an alternative approach to treat patients with Afib in order to avoid the potential negative side effects associated with AADs. Electric cardioversion is a medical procedure that involves delivering a synchronized electrical shock to the heart to restore its normal rhythm. However, this procedure has not been very successful for long-term restoration of the sinus rhythm (18). Catheter-based ablation is a surgical procedure which aims to isolate and possibly destroy abnormal foci responsible for atrial fibrillation. Typically, the treatment involved either a thermal or non-thermal ablation approach. The most common thermal approach is in the form of radiofrequency (RF) ablation, followed by high-intensity focused ultrasound (HIFU) or cryoablation. More recently, the minimally thermal approach of pulsed field ablation (PFA) has gained prominence. The treatment of symptomatic paroxysmal atrial fibrillation (PAF), catheter ablation is now considered the primary order treatment strategy (19). Radiofrequency ablation (RFA) treatment for AFib reports

higher efficacy than AAD therapy and a reduced reporting of complications (20). The left atrial appendage (LAA) is a common target in AFib therapy due to the prevalence of abnormal LAA firing in patients with recurrent AFib (21). Despite increasing adoption in the clinic, the success rate with RFA varies depending on the patient and the type of AFib present. For the ideal candidate receiving ablation therapy, presenting for paroxysmal Afib, the effectiveness is between 60 and 80%. However, for less than optimal patients, such as a patient with persistent AFib, the success rate lies between 50 and 70% (22). High-intensity focused ultrasound (HIFU) is based on the mechanism of vibration that produces mechanical movement of particles within a medium, which is then converted to heat causing thermal tissue injury. HIFU creates wide and deep lesions (up to 11mm) and it is energy dose-dependent (23). HIFU has been shown to have the ability to target a precisely defined location, for example creating lesions in the cardiac tissue while ensuring the epicardium and endocardium are not affected (24). In comparison to cryotherapy or RFA, HIFU has the ability to easily penetrate soft tissues and can produce an ablation without the need for direct physical contact. This makes HIFU advantageous in situations where a challenging location of the tissue impacts the stability and consistency required for tissue contact. Limitations to HIFU include reported permanent injuries to extracardiac tissue such as the wall of the oesophagus and the phrenic nerve leading to nerve palsy and dyspnoea (25).

Cold ablation or cryotherapy is characterised by the formation of intracellular and extracellular ice crystals which results in apoptosis of the surrounding tissue. These crystals are produced by cryothermal energy that is produced by the injection of refrigerant (such as nitrous oxide) through a fine tube. The refrigerant vaporises at the tip of a cryoablation catheter and freezes the tissue (26). While freezing, the catheter tip adheres to the affected tissue, which enables the application of stable energy delivery. In contrast to RFA, tissue lesions induced by cryoablation maintain the tissue structure, including fibrocytes and collagen (27) and present a lower risk of cardiac perforation or thrombogenicity compared to RFA (28).

The latest approach in the arsenal to treat AFib is Pulsed Field Ablation (PFA). This PFA modality is a minimally-thermal catheter ablation technology that uses high-voltage pulsed electrical fields to ablate tissues through the mechanism

known as irreversible electroporation (IRE). This process is based on the application of high electric fields to a cell leading to the formation of large pores in the cell membrane resulting in cell death. IRE has been used previously in other medical areas such as oncology, and due to the reported increased tissue specificity compared to other approaches, PFA may present a safer catheter-ablation option compared to RFA (29).

Limitations of current treatment approaches

Current therapeutic options are expanding and improving to maximise efficiency and reduce adverse effects on the patient. However, the extensive number of potential targets, variables and parameters associated with the ideal pharmacological and catheter-based interventions create a significant limitation to achieving maximal successful control of Afib. The current variability in applied parameters may contribute to the variable successes reported in the clinic. To facilitate the development of an experimental-based set of parameters to achieve successful treatment at minimal cost, it is essential to design an appropriate testing platform that allows us to refine parameters as well as predict and mitigate potential negative side effects. There is a need to strike a balance between the testing and optimization of the treatments while avoiding the risk to the life and well-being of the patients. The development of appropriate models of Afib is essential not only as a disease model to better understand the mechanisms underlying Afib but also as a therapeutic screening platform to facilitate the testing and development of different treatment options for Afib treatment. The absence of appropriate models for Afib for in vitro and preclinical testing has been an obstacle to developing improved therapeutics. A good model should allow the testing of a broad spectrum of treatments, which would result in the selection of the best option to be included

in future clinical trials. Without these models, only limited information can be obtained, and important side effects can be missed (30,31).

In recent years several research models have been developed to mimic human cardiac atrial fibrillation, each of which can provide different information depending on their advantages and limitations. This review addresses different models available for the study of Afib, highlighting their advantages and disadvantages, relevant publications/outcomes and most common uses.

2. Current experimental models of atrial fibrillation

When choosing the best experimental model of Afib it is important to consider the level of complexity that is required. Not including humans, the highest level of complexity is provided by the animal models (most commonly dogs and pigs), which give an insight into heart function, effects on surrounding tissues, other organ systems and behavioural responses to a pharma test or catheter ablation procedure. The next lower level of complexity is represented by ex vivo isolated heart studies which offer the opportunity to analyse heart tissue mechanisms under controlled conditions, very relevant for local short-term pharma and ablation studies. Finally, the use of in vitro cellular models, both in single-cell mono-cultures of cardiomyocytes or the creation of multi-layered and multi-cellular cardiac tissues provides an insight into the cellular and molecular mechanisms involved in Afib processes and the effect of the potential treatments, allowing the specific study of the changes in cell death and beating patterns. As the complexity of the model increases typically the opportunity for higher throughput testing decreases. Thus, the development and optimisation of treatments require a balanced approach and planning a pipeline of tests across multiple levels.

2.2. In vivo models

Animal models are widely used for drug testing and treatment plan development and optimisation for catheter approaches. The complexity of a whole organism approach with the interaction, provides the closest representation to a human model that can be used, making animals valuable models to study the mechanisms underlying Afib, and highly attractive models for catheter-ablation interventions, as they allow surgical procedures similar to humans (32). Different in vivo animal models are currently available and show many similarities to human Afib studies in terms of benefits but also limitations in terms of costs and ethical regulation.

The most common division is according to their size in small and large animal models (33). Small animal models include mice, rats, guinea pigs and rabbits. The accessibility and ease of generation and manipulation are the main advantages of these models. Small animals provide the ability to generate defined genetic manipulations, with a broad range of transgenic species available, especially in mice (34,35). The models are particularly well suited to the study of channelopathies associated with Afib (36). Guinea pigs and rabbits have been shown to have a calcium current-driven plateau resulting in a longer action potential, making these animals of special interest for pharmacological studies of cardiac repolarization related to Afib (37). In general, the use of small animals for Afib provide information about the underlying signalling pathways that may contribute to Afib, however human Afib pathophysiology is not necessarily very well represented in these models. Thus, they are viewed as a starting point for further investigation.

Large animal models of Afib have facilitated the expansion of the knowledge of the complex nature of Afib but have also proven to be beneficial in both the search for novel pharmacological targets and they provide the correct anatomical structures for the study of clinically important changes in the myocardium and associated vessels (38). For example, Fenner *et al.*(2021), demonstrated the inhibition of small-conductance calcium-activated potassium current by the class I drug NS8593 in horses with persistent atrial fibrillation, providing important information about the complex and heterogenous effect of this drug on the right and left atrium (39). In the study of Wiedmann *et al.* (2020), they found the potassium channel inhibitor A293 to be a potential treatment in porcine model of Afib (40)

Large animal models include goat, sheep, dog, pig and horse and they have many advantages compared to smaller animals (41). Surgical procedures are easier to perform on large animals and the heart mass more closely approximates that found in humans. For this reason, these models are more representative of sustained Afib compared to smaller animal models. In most animal models reported to date, Afib commonly appears together with other cardiac diseases such as deterioration of the atrioventricular valves for example in dog models (42). In horses, some studies report spontaneous Afib with no other diagnosed cardiac diseases, whereas

others report at least one-third of horses with AFib present with other conditions (43), making it difficult to isolate the effects of Afib and the potential effect of the testing treatments. Large animal models' limitations compared with smaller species, include higher maintenance costs, ethical conflicts and the requirement for more complex instrumentation.

Animal models have been widely used to test drugs for Afib treatment, one example is the class II anti-arrhythmic drug azimilide, whose efficacy was tested in preclinical studies in dogs (44) and later shown to be effective against Afib in clinical trials (45). Moreover, animal models have provided important information in the development and improvement of catheter-ablation techniques to treat Afib. Most of these studies target the pulmonary veins (46), but also novel areas involved in Afib development such as the epicardial ganglionated plexi which has been shown to resolve Afib in 4 out of 5 cases (47). Animal models are key in determining the effect of these procedures on other areas of the heart and closely located tissues, such as the phrenic nerve (48) or the coronary veins (49), which based on data to date are spared when using PFA. Several studies have shown comparisons between modalities of ablation, such as PFA and RFA in porcine models (50), highlighting the side effects of RFA such as the development of PV stenosis after ablation, which persists even after 3 months (51).

However, *in vivo* models are far from perfect and have several limitations that should be considered. The heterogeneous and multifactorial nature of Afib (52) and the physiological differences across species, creates the main limitation for *in vivo* Afib models (53). Any animal model reproduces at best only limited components of the pathophysiological spectrum of clinical human Afib. A specific limitation to this cardiac condition is the impossibility so far to produce sustained Afib in animal models, as it is predominantly a human condition. Animal models generally do not exhibit Afib except in the acute experimental setting, typically less than a day in duration (33) creating a significant obstacle when studying the long-term effects of this condition. Another significant limitation is related to the cost associated with the use of animal models. Maintenance, instrumentation, and the ablation process itself are costly and increase even more with the use of large animal models. Moreover, ethical considerations regarding the use of animals for scientific purposes need to be taken into account, and ideally, the number of animals used

should be as low as possible, limiting the therapeutic variables that can be tested. Animal models are a necessary preclinical step to help validate any Afib treatment, so ultimately they will need to be used. However, the key to reducing the limitations and costs would be the correct use of these animal models after a previous screening of a therapeutic in other platforms such as in vitro or ex vivo models. Despite limitations, animal models facilitate the possibility to isolate and study the individual mechanisms of Afib, understanding the effect of genetic risk factors and creating drug and ablation testing platforms. Advances such as the combined work with in silico models or improved genetic modifications in larger animals can be new opportunities to expand the knowledge about Afib.

2.3. Ex vivo models

Cardiac tissue isolated from animal hearts has been widely used for cardiac studies using a range of biochemical, electrophysiological, pharmacological and morphological approaches, particularly related to anti-arrhythmic drug safety (54,55). The extraction of whole cardiac tissue facilitates the complex surgical procedures that are needed for whole animal studies allowing a wider range of tissue to be explored and full access to all heart structures. Nevertheless, these tissue samples still show physiological differences that impede the translation of results into human clinical studies.

Availability of human cardiac tissue is, in general, limited to very small amounts of fresh and viable tissues which are considered surgical waste (56,57). However, these small samples do contribute to the study of mechanisms and effects of Afib therapy (58–60). Using these human-explanted tissues overcomes some of the physiological differences found in animal models but is limited by the amount and complexity of the tissue available; often lacking the multi-layered structures which make them more comparable to conventional in vitro models. These models have the great advantage that they avoid any interference from the autonomic nervous system and interorgan communications, which allows the examination of pure cardiac responses against different interventions. These models facilitate a growing interest as a reliable platform for anti-arrhythmic drug testing (61–63).

Recently, these explanted models have been improved by using optical mapping techniques which offer a high-resolution electrophysiological characterization of cardiac human slices subjected to drugs or gene delivery with viral vectors, showing great potential as a pre-clinical platform for novel therapies (64). Other therapies, such as catheter ablation, have used ex-vivo cardiac models to determine the ablated area produced by a certain ablation modality and have the potential to allow for the testing of a wide array of experimental parameters (65–67).

The use of isolated whole hearts was pioneered by Oscar Langendorff who developed the isolated perfused mammalian heart model in 1895 (68) and since then, it has been widely used and aided our understanding of the fundamental physiology of the heart. This model has been used in physiological studies of Afib to better understand the mechanisms of this pathology in numerous animals including rabbit (69), sheep (70), guinea pigs (71) and mice (72). The setup enables the delivery of different compounds such as dyes to track transmembrane potential, allowing imaging of the re-entry mechanisms in the beating heart (73). Recently, the use of actual ex vivo human hearts has become a reality and 83 human hearts declined for transplant were resuscitated in the Visible Heart® Laboratory, showing pulsatile perfusion and evidence of electrocardiogram rhythm, suggesting the great potential of perfused ex vivo systems previously used with animal hearts (74).

Langendorff heart-perfused systems offer an incredible testing platform for catheter-based therapies, particularly epicardial devices. The presence of a completely accessible beating heart allows the physical position of the catheter into the desired part of the heart. Endocardial devices are also possible to test but are more challenging. Langendorff allows complex processes such as the opening of the catheter inside of the heart and the localization of the electrodes to be tested which is not as easily achieved in vivo. Ablation in perfused systems has been previously reported for ventricular fibrillation(75), however, nothing has been reported for the atrium. This opens a new avenue for investigation for catheter ablation testing before in vivo studies, obtaining important information regarding ablation size and the effect on the conductive properties of the heart.

Despite the advances and potential of the *ex vivo* models for Afib studies, these models are complex and challenging to establish and maintain. Typically, the isolated heart models derive from an animal source, which means they do not fully recreate the human condition. The isolated heart is studied in an environment that does not fully recapture those found in the animal or human body, such as the composition of the blood which is commonly substituted with a surrogate buffer (76). Several molecular processes become less effective after removing the heart from the blood supply, particularly ATP depletion (77).

2.4. In vitro models

The adult mammalian heart is composed of multiple cell types, including cardiomyocytes, fibroblasts, endothelial cells, immune cells and mural cells (smooth muscle cells and pericytes), together with adipocytes and neuronal cells (78). In humans, cardiomyocytes are the dominant cell type by volume (70-80% of the adult heart) and are specialised into atrial or ventricular myocytes which are responsible for the contractile forces of the heart (79). However, fibroblasts, which are essential for maintaining the structural, electrical and mechanical features of the heart are the most abundant cell type in the adult heart (80). *In vitro* models encompass a broad range of options that mimic cardiac physiology and pathology to different extents (Figure 1.2).

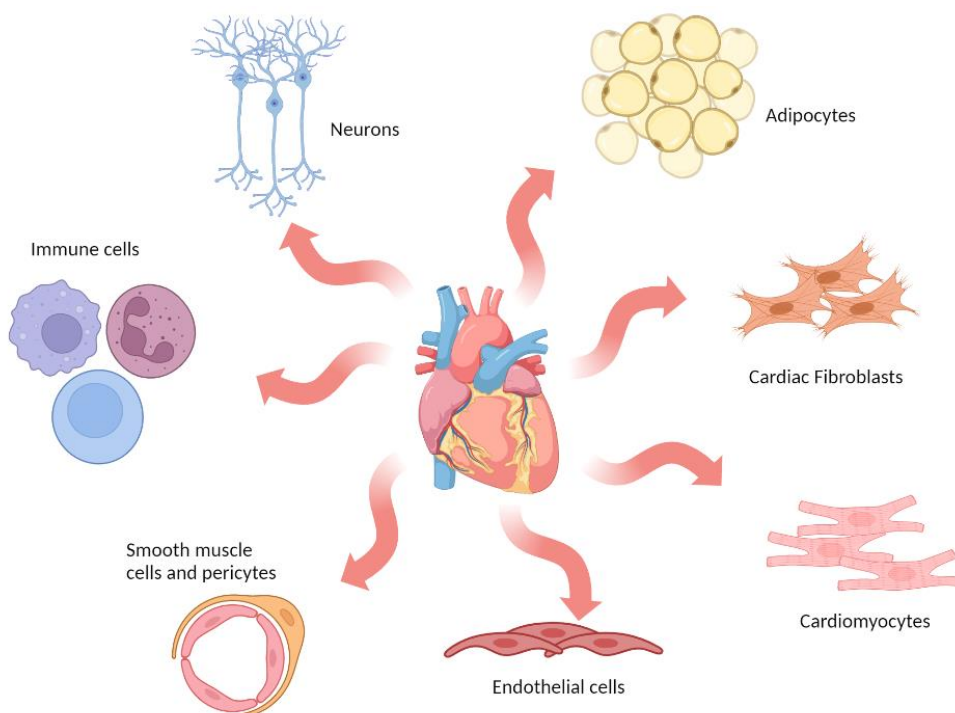


Figure 1. 2. The main cell types in the human heart. The most abundant cell types found in cardiac tissue are indicated in the image. Created with BioRender.com.

2.4.1. Cardiomyocyte-based model systems

Primary cardiac cells have been the most common cells used in the study of cardiac arrhythmias typically in monolayer cultures. Primary adult cardiomyocytes present with a mature ion channel population and sarcomeric structures which are ideal for electrical (81,82), contractility (83) and calcium dynamic studies (84–86). However, they are complex to maintain in culture and show limited capacity for experimentation, as they can only be maintained in culture for a short period of time after being isolated. The isolation process can also be challenging and contamination with other unwanted cell types is common (87). To overcome these limitations, immortalised cell lines have been developed, normally obtained by introducing an oncogene that sustains active cell proliferation. HL-1 cells are an immortalised cardiac cell line established from an AT-1 subcutaneous tumour excised from an adult mouse (88) and have been used for the identification of specific proteins and regulatory pathways involved in Afib-related atrial remodelling such as calpain (89), ER stress-associated autophagy (90), and more general features of Afib (91). The immature H9c2 cell line was originally derived

from embryonic rat ventricular tissue (92) and are widely used in hypertrophy studies related to heart failure (93,94). The most recently developed cell line is AC16 cells, derived from primary human ventricular cardiomyocytes fused with SV40 transformed human skin fibroblasts (95), and have been used to study cardiac hypertrophy, oxidative stress and mitochondrial dysfunction (96–98).

Over the last decade, the emergence of induced pluripotent stem cell (iPSC) technology has greatly advanced our understanding of patient-specific molecular mechanisms of disease and serves as a platform for the development of new therapeutics and drug screening (99). This technology is based on the ability to reprogram disease-specific patient fibroblasts by forcing the expression of specific transcription factors (Oct4, Sox2, cMyc, and Klf4), resulting in a pluripotent state (100). Subsequently, these pluripotent cells are then differentiated into specific mature cells of interest (101). This approach has the advantage of maintaining the patient's complete genetic background and allows the impact of certain key mutations on pathophysiology to be studied. iPSC have been differentiated into cardiomyocytes through a broad variety of protocols (102) and they have provided new insights into the molecular mechanisms of cardiac diseases (103). The advantages and limitations of patient-derived cardiomyocytes have been extensively reviewed elsewhere (104).

In vivo tissues are not composed of only one cell type, so the inclusion of 2 or more cell types in the same system, known as a co-culture has been shown to offer many advantages when simulating the native tissue (105). Cardiac tissue has a heterogenous and diverse cell composition. Atrial tissues contain mostly cardiomyocytes and fibroblasts together with other less abundant cell types such as smooth muscle, endothelial and immune cells (78). It has been reported that essential crosstalk through soluble factors between the cardiomyocytes and fibroblasts is vital for the correct functioning of the cardiac tissue but also can become pathogenic during injury, resulting in a general impairment in electric conduction (106,107). The ability to include several cell types together in the same space makes the co-culture an attractive model to understand the complex interactions between these cell types and their involvement in AFib (108,109).

2.4.2. Adherent cell (2D) models

Adherent cell, monolayers or 2D culture is the most common type of in vitro model system. The process is based on cell seeding over a substrate that facilitates growth and proliferation in a 2D culture format. These models are attractive because of their ease of use and cell growth, manipulation and imaging which allows for an increased number of replicates and higher throughput. 2D culture is well established and reported, with a broad number of studies to compare results (110). In conventional 2D cultures, the whole cell population has even contact with the nutrients and growth factors present in the medium, which results in homogenous growth and proliferation (111). Numerous discoveries have been made by using this simple platform, such as the importance of inflammatory processes (112) and the identification of potential drugs such as pioglitazone, offering the advantage to study and understand the underlying molecular mechanisms of these processes (113). Moreover, cell monolayers can be electroporated and the ablation area can be measured, showing the potential for preclinical testing of ablation devices for AFib therapy (114).

Despite the obvious advantages, 2D systems have certain cell and tissue features that differ appreciably from an in vivo system. One of the most negative examples is the different morphology and organization that cells acquire in vitro compared to that found in the native tissue. This shows the importance of the 3D environment and extracellular matrix that is missing in 2D systems. In order to overcome these limitations and create a smaller gap between 2D in vitro models and in vivo models, some improvements to the classic 2D system have been made.

Cells respond to geometrical and mechanical patterns present in their environment, and the use of cellular micropatterning provides an opportunity to overcome the lack of such patterns when using the standard tissue culture system (115). Micropatterning is a technique which allows the position of cells in specific areas of a substrate, enabling the control of cell shape, position and tissue architecture (116). Several methods can be used to this aim, such as the use of polymers as a stamp of the desired microstructure (soft lithography) (117) or using deep UV through photomasks (photolithography) (118). Numerous studies have taken advantage of this technique to create cardiac fibers in vitro to closely mimic

the cardiac tissue (119,120). Important features such as calcium handling, action potential firing, and conductional velocities are more similar to adult mouse myocardium in micropatterned cultures compared to traditional monolayer cultures (121). The use of iPSC together with micropatterning recapitulates the in vivo atrial conduction using a 1D spiral pattern (122), overcoming the slow conduction present in other iPSC models of Afib (123).

2.4.3. 3D cell culture models

The complex three-dimensional cell structure found in tissues and organs is a key factor for cell function. The strong influence of their morphology through interactions with other cells and the extracellular matrix ultimately influences the whole tissue architecture and function. This 3D microenvironment is essential in cardiac tissue due to the importance of the cell distribution in the muscle fibres to allow the contractions of the myocardium. The use of cell monolayers on rigid plastic culture dishes does not allow the cardiac cells to perform physiological contractions, which is a crucial feature of cardiomyocytes in vivo (124).

In the last few decades, in vitro studies have tried to overcome this limitation by generating 3D models that can closely represent the physiological behaviour of the cardiac tissue. However, the main focus of these models is in regenerative medicine, focused on cell replacement after cardiac infarction (125). The number of 3D cell culture systems reported is increasing and the utility of the models is improving. The use of novel tri-dimensional in vitro techniques opens new insights into the physiological and pathological processes in heart tissue, making them attractive treatment screening platforms. So far, numerous 3D in vitro models have been developed with different levels of complexity, such as cellular hydrogels and engineered heart tissues (EHTs), organoids and organs-on-a-chip.

3D hydrogels

Hydrogels are crosslinked water-soluble polymers that allow the incorporation of cells embedded into the gel tri-dimensional structure. The porosity of the hydrogel allows molecules such as growth factors, nutrients or drug loading

inside the hydrogel (126) and interaction with seeded cells. The first 3D hydrogel culture studies were based on single compounds such as collagen type I scaffolds (127) but have been rapidly updated by the addition of several components of the extracellular matrix such as fibrinogen or basement-membrane matrix such as Matrigel® (128).

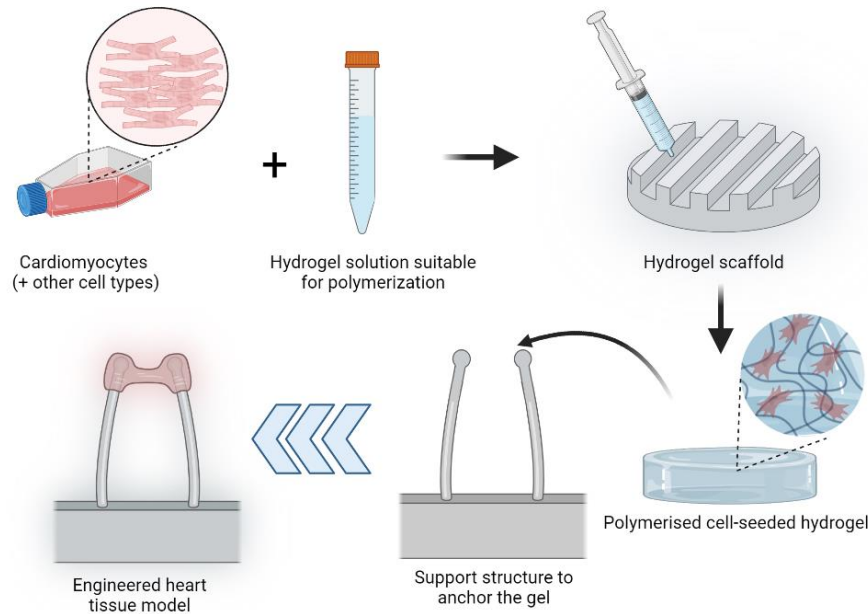


Figure 1. 3. EHTs model production process. Cardiomyocytes alone or together with other cell types (such as fibroblasts) are resuspended in a hydrogel solution that can be polymerised. This mix is added to a scaffold with the desired shape and polymerised to obtain a cell-seeded hydrogel. This hydrogel is further placed in a support structure to anchor the gel. An example of a commonly used support structure is shown above to allow the contraction of the cardiomyocyte-seeded hydrogel. Created with BioRender.com.

Hydrogels have been widely used to develop engineered heart tissues (EHTs), which are tri-dimensional muscle constructs made from isolated cardiomyocytes of different animals, hESC and hiPSC, first described in 1997 (127,129). The elements needed to produce an EHT are cardiac cells, a liquid hydrogel that can be polymerised, a scaffold that will determine the overall EHT shape and a support structure to which the hydrogel will be anchored or attached to (Figure 1.3). Different modifications have been studied to the support structure over the years, such as the use of stretching devices to promote hypertrophy and improved contractile function (130) or two elastic silicone posts to allow auxotonic contractions of the EHT (128). EHTs have the ability to perform contractions thanks to the structure of the hydrogel and the interaction between the cardiomyocytes,

showing organised sarcomeres and defined beating patterns (131). These processes, together with electrical stimulation are key for the further maturation of the hiPSC-cardiomyocytes (132). Recently, the inclusion of other cell types such as fibroblasts helped create a closer representation of the cardiac tissue (133,134). Furthermore, atrial and ventricular EHTs can be designed and have shown different features with similarities to that seen in vivo, allowing a highly specific model for the study of cardiac pathologies such as Afib (135).

EHTs have a great potential for preclinical therapeutic screening, as drug screening platforms (136) and are increasingly valuable models to test ablation-related therapies (Figure 1.4). Hydrogels can be designed to be temperature-sensitive which would help to predict possible thermal damage risk of a given set of parameters and set up before further animal and clinical studies (137,138). They provide information that, working together with in silico models, can help to predict and plan therapeutic ablation interventions for AFib, as it has been shown previously for cancer treatment models (139,140).

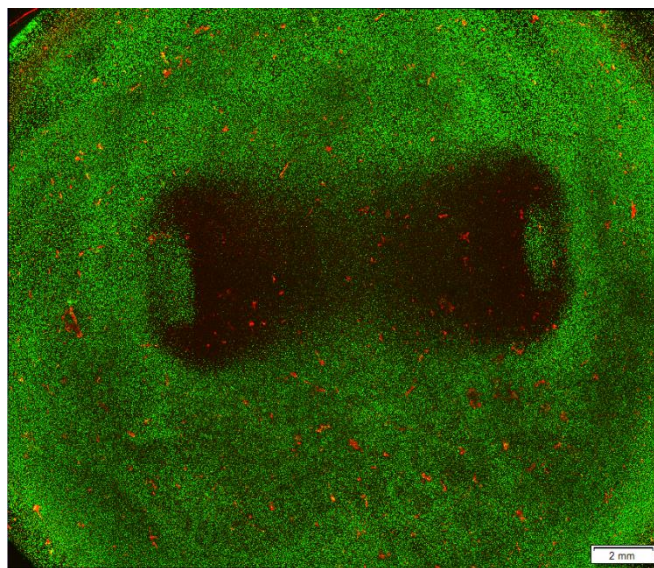


Figure 1. 4. Ablated area after ablation treatment in a Hyaluronic acid hydrogel model seeded with cardiomyocytes. AC16 cardiomyocyte cell line was seeded in a hyaluronic acid hydrogel model and treated with 36,000 biphasic pulses of 2 μ s duration and 1250V of input voltage. After ablation, the cells were stained after ablation with live/dead staining, which labels live cells in green and dead cells in red. The image was obtained using a confocal microscope to visualise the lesion area.

3D organoids

Organoids are tri-dimensional, multicellular cultures which are capable of self-organization into complex tissue-like and organ-like structures, supported by an extracellular matrix (ECM). The ability to create these structures is mostly restricted to stem cells, such as pluripotent embryonic stem cells (ESC) or induced pluripotent stem cells (iPSC), which can be further matured into the desired cell phenotype. Other cell types that can create organoids are the tissue-resident adult stem cells (ASC), which are present in adult tissues and show the ability to self-renew and differentiate into other cell types while preserving their tissue specificity (141–143). ASC-based organoids need to be supported by a cocktail of growth factors in the culture media involved in signalling control in vivo tissue conditions.

In recent years, several production methods have been developed, the most common is based on cell seeding over or embedded into a matrix such as Matrigel® (an ECM protein mix), which provides an appropriate environment. This method allows the monitoring of processes such as cell adhesion, migration, and chemotaxis (144). The use of spinning reactors allows batch production of organoids with larger sizes. Cells are placed in a container which is constantly stirred to avoid cell attachment (145). The hanging drop method has been used for decades, taking advantage of gravity to induce cell aggregation and assembly in a droplet of medium typically hanging from the lid of a culture dish. This approach was enhanced by the use of hanging drop plates (HDPs), creating an array of spheroids (146). Other methods employ non-adherent surfaces to cultivate the cells, facilitating them to form aggregates and eventually make spheroids, which is a simple method with high throughput and more cost-effective than other methods (147,148). Magnetic nanoparticles have also been employed, relying on the fact that they are taken up by the cultured cells, allowing them to float in the media and favouring its aggregation and production of ECM (149). Finally, the use of bioprinting for organoid formation has gained increasing interest in the last 5 years (150) This technique allows precise control of the shape and distribution of the ECM and organoids, enabling a better representation of the in vivo environment. Bioprinters' function is based on additive manufacturing, which deposits the desired material layer by layer until reaching the final desired structure (151).

Human cardiac organoids have a huge potential as disease models for heart disorders. They have the capacity to produce spontaneous and induced electrical activity, showing higher conduction velocities than 2D cultures. Cardiac organoids can help the study of complex electrical arrhythmic processes such as re-entry, hereditary arrhythmias and personalised medicine using hiPSCs. Shinnawi *et al* (2019). created a cardiac organoid model based on hiPSCs from patients with the arrhythmogenic syndrome known as short QT syndrome. This model showed a similar development of re-entry arrhythmia as seen in patients with this syndrome. This study provides evidence of the ability of cardiac organoids to recapitulate disease phenotype and new insights into the mechanisms underlying this arrhythmia syndrome.

Despite the significant potential of organoids for disease modelling and drug screening, some limitations still need to be addressed. Organoid cultures show differences in gene expression patterns when compared with the *in vivo* tissues they are trying to mimic (152). Organoid cultures show a high heterogeneity of cell phenotypes, containing various clones in different proportions, which makes the study of specific mutations difficult (153). The absence of vascular and immune systems in organoid cultures make the representation of the tissue microenvironment difficult (154), as well as presenting significant ethical regulation challenges regarding the use of hiPSC (155).

Organ-on-a-chip and microfluidics

Organs-on-chips are systems containing engineered or natural microtissues grown into microfluidic chips, designed to control cell microenvironments and maintain tissue-specific functions. The microfluidic chip contains networks of hairline microchannels for guiding and manipulating small volumes of solution (156). They allow the ability to control parameters such as concentration gradients, cell distribution or tissue-organ interactions (157–159). Depending on the questions being asked this approach allows a single-organ system if the aim is the evaluation of the response of a specific organ to a compound(s) or multi-organ system to study the interaction between organ systems, usually via exchange of metabolites and other soluble molecules, they are commonly known as body-on-a-chip (160).

Arrhythmia has not been widely modelled in organs-on-a-chip so far, but some studies report promising results in replicating the cardiac microenvironment (161).

3. Future perspectives and challenges in atrial fibrillation modelling

Current therapeutic options do not fully address the clinical need to improve Afib therapy, and one of the potential reasons for that is the lack of appropriate preclinical models to sufficiently support a broad array of test parameters, and treatment efficacy assessment and allow safety testing. Due to the complexity of factors involved in Afib, the differences between species and the regulatory processes involved in the use of animals and their organs, the choice of the best preclinical model is a challenge that can be key to the success of the treatment in the clinical scenario. In vitro models have undergone a revolution in the last number of years, especially with the arrival of iPSC technology and complex 3D culture systems. Improvements are required to obtain completely mature patient-derived cardiomyocytes, combined with the efforts in optimising 3D models and EHTs such that we can create a useful preclinical model for high throughput testing of both pharma and device-based innervations. The inclusion of multiple cell types, creating a similar environment to in vivo would provide the influence of the crosstalk between different cell types, which is essential in the functionality of the heart. In the future, these models could be combined together with perfusion, creating the idealised tri-dimensional in vitro, a patient-specific heart that would allow the testing of the anti-arrhythmic therapies in advance or the clinical procedure being performed. This allows clinicians to plan and optimise the best treatment modality for each individual patient and mitigate risks.

Chapter 2 – Electroporation Parameters for Human Cardiomyocyte Ablation In Vitro

Following the detailed review of the current models of Afib, and their advantages and disadvantages as therapeutic platforms, there is a demand to design better in vitro models to develop selective and effective treatments for Afib. To this aim, this chapter explores the potential of two simple in vitro models (cell suspension and monolayer) that can be used as early screening models for ablation therapy of Afib. These models offer the simplicity to produce of a large amount of data that will help reducing the parameter options in more complex in vitro models and in vivo studies.

1. Introduction

Atrial fibrillation (AFib) is the most common category of cardiac arrhythmia reported in humans characterised by sporadic atria hyperexcitation resulting in dyssynchronous atrial contraction and irregularity in ventricular excitation (162). AFib is an increasing global health problem as its prevalence is on the rise, with an estimation of 33 million people worldwide diagnosed with AFib in 2020 which is expected to double by 2050 (2). AFib patients typically present with high morbidity and mortality rates because of the severe consequences associated with thromboembolism and stroke (3). Moreover, in the last 2 years, infection with COVID-19 is reported to be associated with a more frequent occurrence of arrhythmias (4), making AFib a global issue thus placing a strong demand for efficient and effective ways to deliver appropriate AFib therapy.

Classically AFib can be divided into paroxysmal, persistent, long-standing persistent, or permanent, depending on the duration of the symptoms. Paroxysmal AFib resolves typically within 7 days of onset while persistent AFib is sustained for longer than 7 days. Long-standing persistent AFib lasts more than 12 months and permanent AF is used when there has been a joint decision by the patient and

clinician to cease further attempts to restore or maintain sinus rhythm (163). Despite the sub-classifications, the pathophysiology underlying AFib is not yet fully understood. A key component in the maintenance of the AFib arrhythmia is the process of re-entry, which occurs when impulses travel in an abnormal repetitive circuit (164). This trigger that initiates the arrhythmia is commonly an ectopic firing focus. The first reported focal ectopic firing was found within the pulmonary veins (PVs) in patients with paroxysmal AF; ablation of these ectopic foci has been shown to reduce AFib burden, demonstrating a role for PVs in AFib (6). Several subsequent studies have provided support for the role of PVs and cardiac ganglionated plexi in AFib initiation and highlight them as targets for therapeutic ablation (7–9,165).

Catheter-based pulmonary veins isolation (PVI) is now an established treatment option for AFib. Thermal ablative approaches with either radiofrequency (RF) or cooling (cryotherapy) technologies suffer from collateral damage effects to adjacent structures including the wall of the oesophagus and the phrenic nerve. These issues have resulted in alternative technologies to be considered such as irreversible electroporation (IRE) (166–168). The delivery of nano- to milli-second electrical pulses which is minimally thermal in nature alters cell membrane permeability leading to cell death. Cardiac ablation with IRE has yielded some positive data including a selection of human studies (49,169–174). There are several unanswered questions regarding the fundamentals of IRE ablation as applied to cardiomyocytes. Previous work from this lab and others has established threshold parameters for IRE with cardiac tissue but has focused on either immature cardiomyocytes or cells from rodent models (175,176).

The goal of the current study is to assess electroporation ablation thresholds in human cardiomyocytes in suspension and 2D culture. These two in vitro models are optimised and the process of ablation is studied in each model by applying selected pulse parameters and analysing the outcomes using fluorescence. This work provides essential insights into the underlying selectivity of IRE and can be quickly translated to clinical applications.

2. Materials & Methods

Cell culture

Human cardiomyocyte cells AC16 (Sigma-Aldrich) were cultured in T75 flasks and passaged with trypsin-EDTA 0.025% (Sigma-Aldrich) every 2-3 days for maintenance. Cardiomyocytes were cultured in Dulbecco's Modified Eagle's Medium/Ham's Nutrient Mixture F-12 (DMEM/F-12) (Sigma Aldrich) supplemented with 12.5% Foetal Bovine Serum (FBS) (Gibco), 1% Penicillin/Streptomycin (Sigma Aldrich) and 2 mM L-Glutamine (Sigma Aldrich). For adherent cell experiments, 6 well plates were coated with 0.1 mg/ml gelatin before cardiomyocytes were seeded with a cell density of 7.5×10^5 cells per well overnight to ensure complete confluence. For cell suspension experiments, 1×10^5 cells were used per cuvette.

Immunocytochemistry and staining

Cardiomyocytes were fixed with 4% paraformaldehyde for 20 minutes and blocked with 0.2 % bovine serum albumin (in 0.1% Triton-X100) for 1 hour at room temperature. Cardiomyocytes were incubated with Troponin I, clone 1F23 ZooMAb Rabbit Monoclonal Antibody (Sigma-Aldrich) in blocking solution at 4°C overnight. Primary antibodies were aspirated and incubated with anti-rabbit 488 fluorophore conjugated secondary antibody (Abcam, 1:1000) and DAPI (Sigma-Aldrich) in blocking solution for 1 hour at room temperature. Cells were imaged using EVOS M7000 microscope system (Thermo Fisher Scientific).

Electroporation protocols

Cardiomyocytes were exposed to a typical Irreversible Electroporation (IRE) protocol consisting of a 100 μ s duration biphasic pulse, delivered in bursts of 5 pulses per burst. Increasing electric fields were generated using the Gemini X2 Twin Wave Electroporation Generator (BTX) together with the Safety Dome (BTX) and the electroporation cuvettes (4 mm gap) for suspension experiments (Figure

2.1A). In addition, in some experiments we used custom electrical field protocols applying 2 μs or 5 μs pulses produced by biphasic generator (RBC Medical Innovations). To ensure operation with safe limits with this generator, the stimulation pattern was delivered in 100 or 250 bursts, with each burst containing 60 pulses. For cell suspension studies, field strengths ranged from 0-1500 V/cm. For adherent studies an input voltage of 600 V was chosen as a field strength that was above the ablation threshold and was delivered to the cells directly into the culture well plate using a custom-printed probe for ablation (Figure 2.1B) with electrode size (3x5 mm with a 1 mm fillet, 50 μm in thickness) and the edge-edge gap of 5 mm. For the ablation studies, the electrodes were placed 1 mm above the cell layer and covered in DPBS solution. The different ablation protocols and attendant on-times are presented in Table 2.1.

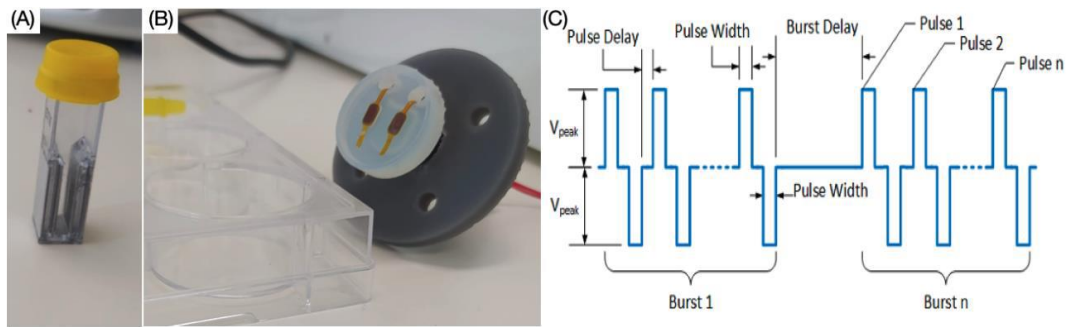


Figure 2. 1. Electroporation equipment for ablation experiments. (A) Cuvette with 4 mm gap. (B) Adherent cell custom-printed probe. (C) Biphasic pulse waveform.

Table 2.1. Ablation protocols applied to different models of cardiac cell culture

Ablation protocol	Pulse width (μs)	Pulse number	Burst number	On-time (ms)
1	100	5	3	3
2	100	5	60	60
3	2	60	100	24
4	2	60	250	60
5	5	60	100	30
6	5	60	250	75

Live-Dead assay

Measurement of cell death in cell suspension experiments was performed by incubating the cells 2h post-ablation with 3 μM propidium iodide (PI, 30 minutes, 37°C) (Sigma-Aldrich). PI is a red-fluorescent nuclear counterstain which is commonly used to detect dead cells by binding to their DNA. The PI signal was measured using Hidex microplate reader (Hidex Sense) at an excitation/emission of 520/620 nm.

Ablation images in adherent cell experiments were assessed by incubation with 3 μM PI and 1.5 μM Calcein-AM (30 minutes, 37°C) (Sigma-Aldrich) and images were obtained by scanning the wells using EVOS M7000 Imaging System. Images were analysed using NIH ImageJ to determine the ablation parameters: area, perimeter, and Feret Max diameter (Fmax).

Numerical modeling of 2D ablation parameters

A simplified numerical model of the experimental setup was designed in COMSOL Multiphysics® 5.6. The computer-aided design model contained the simplified resin printed probe, the polyimide insulation behind the electrodes, the copper electrodes. In the well, a 100 μm thick layer (34.8 mm in diameter) was used to represent the cell layer and the probe rested ideally on top of this layer. The 100 μm thickness was chosen based on dimensions of ventricular cardiomyocytes cells given in Vu and Kofidis, (2014) (177). On top of the cell layer, a layer was drawn for DPBS (7 mm in height). As the conductivity of the cell layer was unknown, the conductivity of DPBS was assigned. The conductivity of DPBS in the model is estimated at 1.2-1.6 S/m (178). The terminal and ground boundary conditions were assigned to the boundary at the bottom of the electrodes. The applied voltage at the terminal was 600 V. The very high and very low conductivity materials were replaced as boundary conditions in the model at the material interface of the DPBS and cell layers. In this case, the current was not expected to flow through the sides or back of the electrodes where polyimide insulation was used in the real-world setup. Also, the current was not expected to flow through the low conductivity plastic

probe. The electrode was assumed to have equal potential across the surface. The boundary conditions elsewhere were assumed to be perfectly insulated. The discretisation was then performed for the DPBS layer and the cell layer. A tetrahedral element mesh of approximately 1.88 million elements was used to mesh model. Similar to previous work by Wasson *et al.*,(2020) the conductivity within the model was assumed constant (140). A stationary study was run with the Electric Currents Physics in the AC/DC module.

Statistical analysis

All data were analysed using one-way and two-way ANOVA and multiple comparison tests using IgorPro Ver. 9. Experiments were repeated for at least three independent experimental blocks with three technical replicates (N=9). Statistical analyses were performed with a confidence level of $\alpha = 0.05$.

3. Results

3.1. Effect of electric field parameters on cell death in suspension culture

AC16 cells stain positive for human troponin I, confirming the human cardiomyocyte phenotype marker (Figure 2.2A). In suspension culture, cardiomyocytes were exposed a standard biphasic waveform consisting of 100 μ s negative followed by 100 μ s positive phase with different electric field strengths (250, 500, 750, 1500 V/cm). In addition, the pulse number was varied using either ablation protocol 1 or 2 (Table 1) which is the equivalent of an on-time of 3 ms or 60ms respectively. For 3ms on-time cardiomyocyte viability was statistically significantly reduced after exposure to fields greater than 750 V/cm up to a maximum of 30% cell death at 1500 V/cm (Figure 2.2B). While 60 ms on-time resulted in significantly increased cell death at all field strengths (Figure 2.2C). If we define the optimal ablation threshold as the minimum electric field and on-time resulting in 70% cell death we can see that the threshold for cardiomyocytes is 500 V/cm with an on-time of 60 ms (Figure 2.2C). Based on this criterion, smaller

numbers of pulses are equivalent to a lower on-time and while this may limit the potential risk of collateral damage it also reduces the effectiveness of the IRE to ablate cardiomyocytes. Longer (60ms) on-time results in effective cell death across a range of field strength, however, this also increases bubble formation and thermal effects. Hence higher voltages >750V/cm are not included in our analysis (Figure 2.2C below).

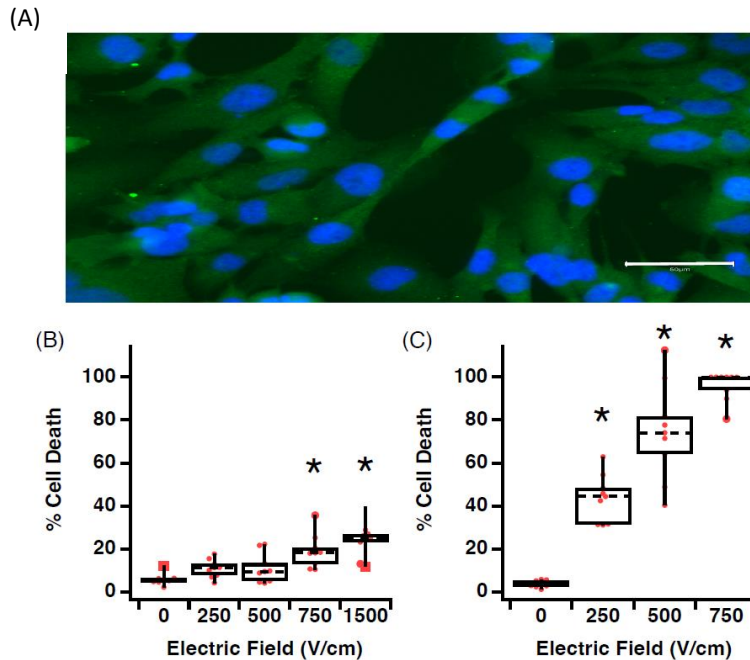


Figure 2.2. Increasing electrical field strength increases cell death in human cardiomyocytes. (A) AC16 cells in culture stained positive for phenotypical markers of human cardiomyocytes, scale bar 50 μm . (B) Effect of field strength on cell death with a 3 ms total on-time. (C) Effect of field strength on cell death with a 60 ms total on-time. Data are representative of at least 3 independent experiments and plotted as Max, Min and Median. ** $P < 0.05$, One-Way ANOVA, Dunnett's post-hoc test.

The literature suggests that shorter pulse durations in the micro or even nanosecond domain may reduce the rise of hydrolysis and arcing (179). To examine the effectiveness of short pulse durations on cell death, we compared 2 μs versus 5 μs pulse durations using biphasic waveform for 100 (ablation protocol 3 and 4, Table 2.1) or 250 bursts (ablation protocol 5 and 6, Table 2.1) in suspension culture. Application of 2 μs pulses resulted in significant cell death at electric fields of 750 V/cm and above (Figure 2.3A). In addition, at 1000 V/cm and 1250 V/cm, 250 bursts resulted in significantly (** $p < 0.005$) more cell death than 100 bursts and this differential disappeared at 1500V/cm. In line with previous data, increasing pulse duration from 2 μs to 5 μs increases cell death overall (Figure 2.3B above).

The difference observed when jumping from 1000V/cm to 1250V/cm, is also significantly higher (** $p < 0.005$) for 250 bursts and more effective at causing cell death than 100 bursts (Figure 2.3B). In comparing across treatment groups, a field strength greater than 750 V/cm increases cell death, independent of pulse duration or burst number applied (Figure 2.3C). However, it is also evident that at higher burst numbers (250 bursts) there is little effect of pulse duration at voltages greater than 750 V/cm. Using lower burst numbers (100 bursts) at 750, 1000 and 1250 V/cm we see statistical differences in percentage cell death with the 5 μ s pulse more effective than 2 μ s pulses (Figure 2.3C).

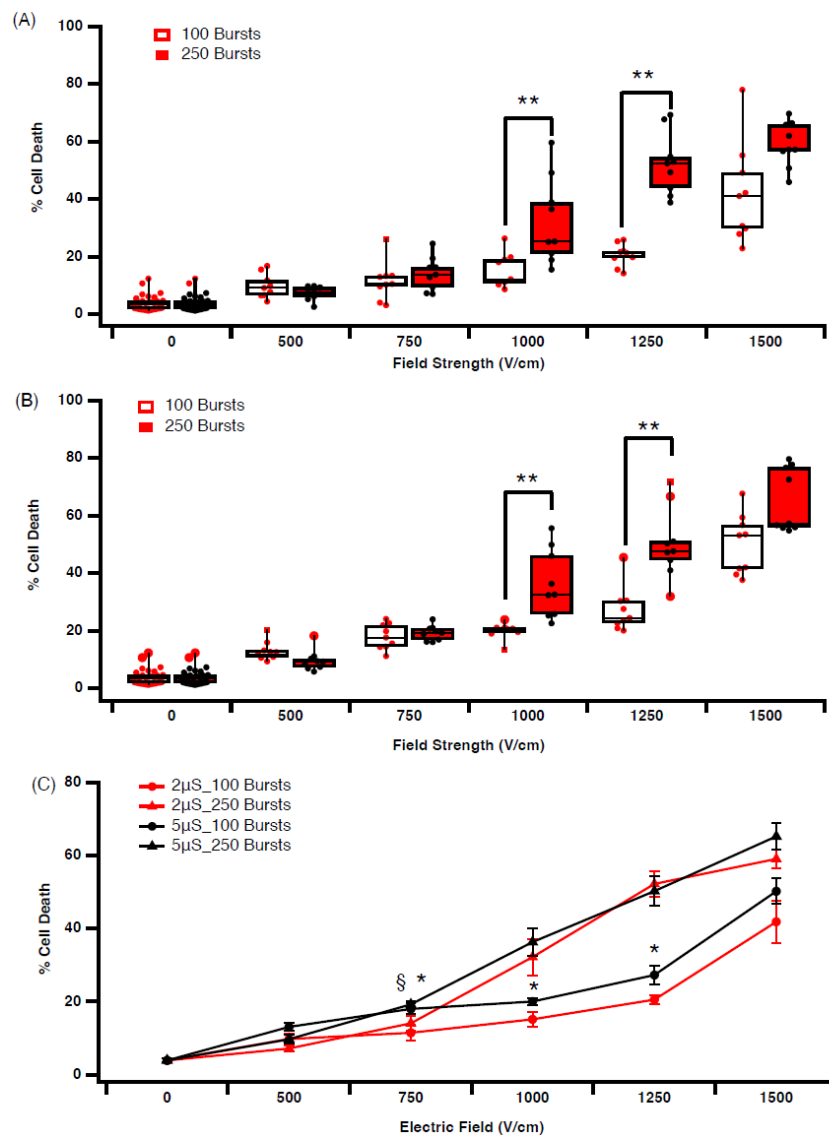


Figure 2. 3.. Increasing pulse duration, burst number and field strength reduces cardiomyocyte viability. (A) Effect of 2 μ s pulse duration on cell survival. (B) Effect of 5 μ s pulse duration on cell survival. (C) Comparison of 2 μ s versus 5 μ s pulse duration on human cardiomyocyte survival. Data are representative of at least 3 independent experiments and plotted as Max, Min and Median. ** $P < 0.05$, One-Way ANOVA, Dunnett’s post-hoc test.

3.2. Effect of time on cell death and lesion size in a 2D culture model

Cells were grown in wells to near full confluency in this 2D model. Cells were exposed to a lethal ablation threshold established in earlier experiments and live-dead analysis was assessed with propidium iodide (PI) staining at 0.5, 2 and 24 hrs post electroporation. Exposure to a 2 μ s pulse at 600 V/cm with 100 or 250 bursts (ablation protocol 3 and 4, Table 3.1) results in increasing time-dependent cell death, with 250 bursts always resulting in more cell death at each time point (Figures 2.4A). The ablation area, Fmax and ablation perimeter (Figure 2.4B, C and D) all increase significantly with 250 bursts compared to 100 bursts. No significant difference over time with higher pulse numbers. However, at 100 bursts we see a significant increase in all parameters measured 24 hours post-ablation was observed. This indicates a possible delay in cell death pathway activation by IRE, which is masked when higher burst numbers are applied. Most likely this is due to the activation of apoptosis pathways which are activated by IRE and take more than 2 hours to execute their program (Figure 2.4B, C and D).

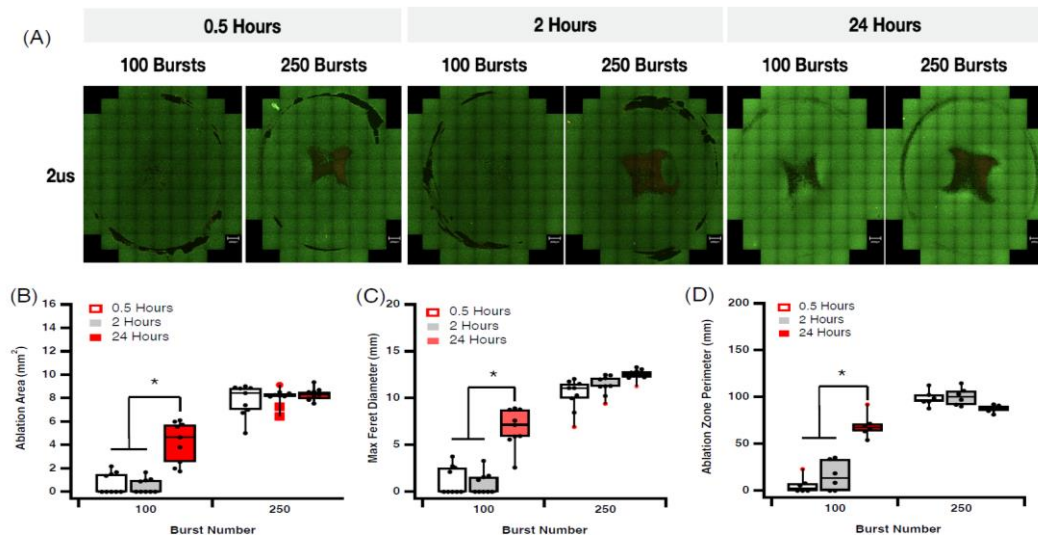


Figure 2. 4. Effect 2 μ s pulses and burst number on cardiomyocyte lesion size. (A) Effect of 2 μ s pulse duration on cell survival. (B) Effect of burst number over time on ablation area. (C) Effect of burst number over time on max Feret diameter. (D) Effect of burst number over time on ablation zone perimeter. Data are representative of at least 3 independent experiments and plotted as Max, Min and Median. **P < 0.05, One-Way ANOVA, Dunnett's post-hoc test.

A similar pattern of lesion formation is observed for 5 μ s pulses (ablation protocol 5 and 6, Table 3.1) in our 2D model. Increasing burst number increases cell death, ablation area, Fmax and the ablation perimeter (Figure 2.5). At the higher field strengths, the time dependent increase in cell death is not significant, in contrast to that observed at 2 μ s (Table 2.2). While increasing pulse amplitude (2 μ s versus 5 μ s) and increasing burst number (100 versus 250) results in greater ablation area (Figure 2.5A & B), Fmax (Figure 2.5C) and ablation zone perimeter (Figure 2.5D), these data suggest two different cell death mechanism are at play. Time-dependent changes are only observed at the lower pulse amplitudes suggesting that higher intensity electric fields with shorter duration on-time may allow more controlled cell death. This trend is consistent with the profile of field contours demonstrated in the in-silico model we generated. The ablation zone associated with our IRE treatment was simulated using COMSOL Multiphysics software (Figure 2.6). Based on our data we predict that cell death via necrosis is occurring in the proximity of the epicentre of the electric field, with predicted field strength close to 900V/cm. As the electrical field drops off toward the periphery other forms of cellular response are anticipated including apoptosis and reversible electroporation.

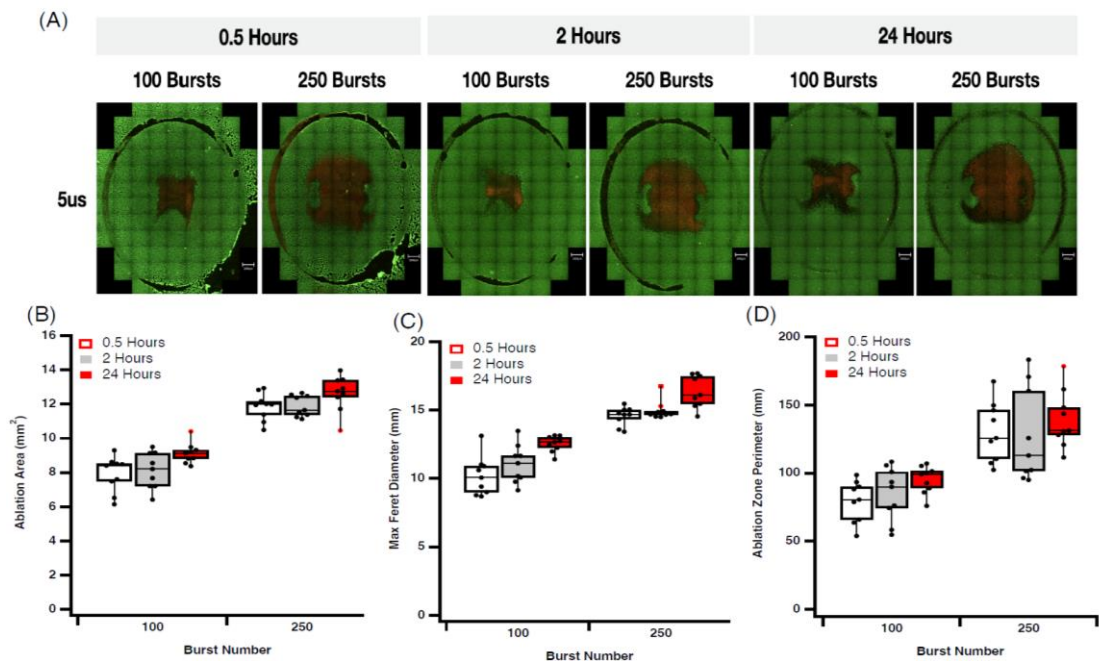


Figure 2. 5.Effect 5 μ s pulses and burst number on cardiomyocyte lesion size. (A) Effect of 5 μ s pulse duration on cell survival. (B) Effect of burst number over time on ablation area. (C) Effect of burst number over time on max Feret diameter. (D) Effect of burst number over time on

ablation zone perimeter. Data are representative of at least 3 independent experiments and plotted as Max, Min and Median. ****P < 0.05**, One-Way ANOVA, Dunnett’s post-hoc test.

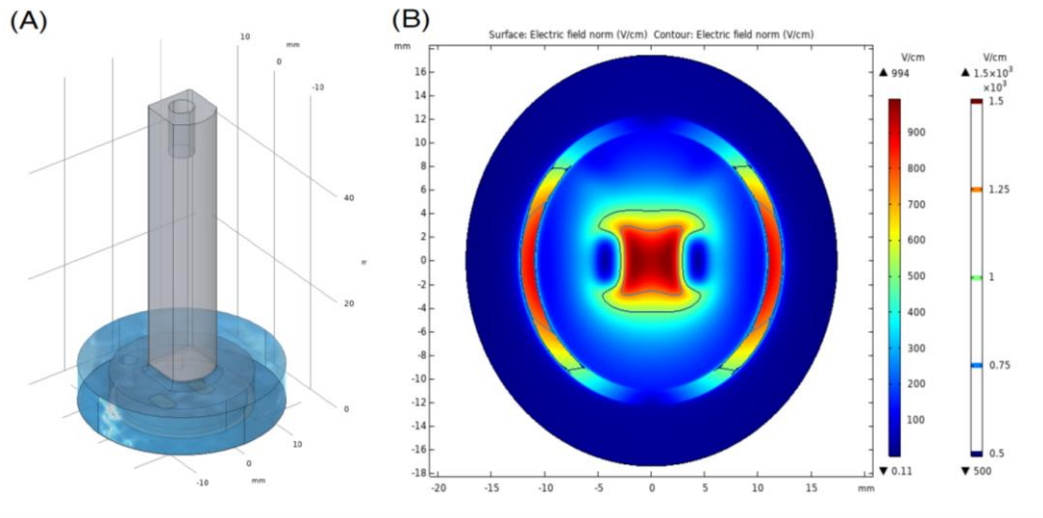


Figure 2. 6.The numerical model and the electric field strength plot of the 2D electroporation at half the cell layer thickness of 50 μm .

4. Discussion

The data clearly demonstrate that human cardiomyocytes are susceptible to damage and cell death from electroporation across a range of pulse parameters which suggests there is significant room for optimisation in clinical IRE application. At a cellular level, IRE results in the formation of hydrophilic nanopores in the cell membrane. At higher intensity these changes are permanent having long-lasting/irreversible effects on permeability across the phospholipid membrane (180). In general, the data shows that increasing field strength increases cell death, but importantly, increasing the number of pulses for a given electric field can have significant benefits in terms of ablation. Using a conventional 100 μs biphasic pulse at 500 V/cm with 3 ms on-time (ablation protocol 1) results in approximately 15% cell death. Using the same parameters, increasing only the on-time to 60 ms (ablation protocol 2) results in 75% cell death (Figure 2.2). Others have shown significant IRE induced ablation of H9C2 rat cardiomyocytes at field strengths greater than 375 V/cm (181). While more recently Hunter *et al.*,(2021) reported that biphasic pulses 500 V/cm caused 80% cell death in monolayers of rat ventricular cardiomyocytes (176). However, in this case the authors used a single pulse of 10ms (5 ms for each phase) in stark contrast to our pulse parameters. In a recent review

by Sugrue *et al.*, (2018) where they examined 16 eligible clinical IRE cardiac ablation studies they reported that the pulse duration varied from 20 μ s to 6 ms and the number of applied pulses varied between 1–200 per procedure (182). Thus it is clear that both monophasic and biphasic pulses can be effective, the advantages or disadvantages of either waveform type, pulse duration or pulse number on lesion formation are unclear and requires additional work.

There is increasing interest in applying shorter pulsed electric fields for IRE, using pulses in the nano- and microsecond domains. The concept is that this may further circumvent the limitations of RF- and cryoablation and also reduce neuro and neuromuscular activation. Ablation with nsPEFs has been successfully used for tumours (183), but there is minimal evidence in cardiac tissue (184). Here it is demonstrated that a short pulse of 2 or 5 μ s can be effective in inducing ablation in suspension culture (Figure 2.3) and that altering pulse length and number can facilitate control of lesion size in 2D cultures (Figures 2.4 & 2.5). This is in line with previous work that showed at higher field strength, the percentage of cell damage is greater for mouse cardiomyocytes (176). When comparing ablation protocol with equivalent on-time but different pulse length we see some interesting data. Ablation protocols 2 and 4 have the same on-time but pulse lengths of 100 μ s versus 2 μ s respectively. At a field strength of 500 V/cm protocol 2 results in approximately 75% cell death while protocol for the same field strength results in approximately only 10% cell death. In addition, 750 V/cm protocol 2 results in approximately 100% cell death while protocol for the same field strength results in approximately only 18% cell death. Clearly pulse duration has a very significant effect on cell death.

Furthermore, these data suggest that there is a time dependence to cardiomyocyte cell death and at voltages near the ablation threshold (600V/cm), significant cell death can emerge 24 hours post ablation. While at higher field strength, cardiomyocyte death is more consistent and is less time dependent. We show that a fraction of cardiac cells die almost immediately after the treatment, regardless of the electric field. This type of response was also reported by others for cancer cells (183,185).

In recent years, there has been considerable development in catheter design that supports so-called single-shot applications (Farapulse Inc., Menlo Park, CA, USA), or the more geometrically complex Sphere-9 catheters (Affera Inc. Newton, MA, USA), originally designed for RF but are also able to deliver bi-phasic pulsed electric fields. The investigation of optimal IRE parameters to maximise tissue selectivity and to control the temporal and spatial aspects of lesions is limited. The acute and chronic assessment of lesion durability and/or lesion expansion after IRE needs further investigation. The current data support the idea that appropriate parameter selection can deliver tissue selectivity far in advance of other modalities. This ultimately will improve safety, reduce collateral damage and reduce procedure times in the clinic. However, to fully realise the clinical potential of IRE, this will require the determination of the optimal IRE parameters, and an important consideration in this regard will be the appropriate monitoring time after the application of IRE for the accurate assessment of cell death. Previous studies have pointed out the significance of observational times when carrying out a histological evaluation of the ablated areas in animal models treated with IRE (186).

Cell death pathway activation has been shown to be dependent on a number of variables including field strength and pulse number (187). Predicting the effect of IRE and driving cell death down a particular pathway may have advantages in the clinic by reducing inflammatory and immunogenic responses (188). While this study did not measure cell death pathway activation the 24-hour delay in the response to some IRE waveforms strongly suggests apoptosis was activated and that this may be beneficial as it is associated with less inflammatory responses. It is likely based on this modelling (Figure 2.6) that cells at the centre of the field are dying of necrosis while as the field contours reduce, more subtle changes in cell responses are likely. These responses will include activation of apoptosis and reversible EP from which cells can recover. The model correlates well to the cell death profile in the 2D adherent cell culture model and will provide an important assessment tool for studying changes in field parameters and lesion size. Further studies are required to fully elucidate the effect of conventional IRE on cell death pathways and the tuneable nature of lesion size.

Limitations

In this study, the 2D monolayer culture of human cardiomyocytes facilitated the testing of IRE parameters allowing the iterative exploration of pulse protocols. However, while these AC16 cells are a very close representation of cardiac muscle our model is limited by the lack of 3D geometry. In the present in-silico model, assumptions are made about the conductivity of surrounding fluids and tissues which may differ substantially from native tissues and thus affect the electric field thresholds applied. However, there is confidence that the relative differences observed comparing the various IRE protocols would be representative of the in vivo scenario. Future studies incorporating a three-dimensional model with more representative conductivities are required to allow full extension of identified ablation thresholds to the clinic.

5. Conclusions

The results highlight the potential to tune IRE protocols to achieve efficient and selectively cell death in cardiac applications. Furthermore, the data highlights the potential to minimise inflammatory responses by selectivity inducing cell death through activation of delayed cell death pathways. It is clearly shown that on-time though pulse timing or burst number applied, rather than absolute field strength may be a better predictor of ablation area. These results provide new insight into the field of cardiac IRE but must be explored further to fully extrapolate to clinical outcomes.

Chapter 3 – Optimization of a 3D Hydrogel Model for Cardiomyocyte Ablation In Vitro

In the previous chapter, the 2D monolayer culture of human cardiomyocytes facilitated the testing of IRE parameters allowing the iterative exploration of pulse protocols. However, while AC16 cells are a very close representation of cardiac muscle the model is limited by the lack of 3D geometry. The in-silico model contains assumptions regarding the conductivity of surrounding fluids and tissues which may differ substantially from native tissues and thus affect the electric field thresholds applied. The importance of these parameters and their involvement in the ablation process highlights the need of more complex models to completely understand the effect of PFA. This chapter aims to develop and optimise a 3D hydrogel model with cardiomyocytes, exploring the effect of two potential gels in cell growth, morphology and their utility as ablation models.

1. Introduction

Current 2D in vitro models have proved to be powerful high-output tools to initially explore the effect of waveform ablation parameters on cardiomyocyte cell viability. These models have provided information regarding the ablation area size, how it is distributed around specific electrode geometry, and which parameters are involved in the ablation process. The main purpose of these models is to act as a screening platform to reduce the range of parameters tested when choosing the optimal ablation parameters in further studies. Although the simplicity of these platforms is attractive, they are far from an ideal representation of the complete cardiac tissue structure. One of the main limitations of these models is that they do not correctly reflect the potential effects of tissue geometry on the ablation process, leading to aberrant cell morphology and potentially different reactions to a selected drug or ablation parameter. Other factors such as cell adhesion or nutrient uptake also differ from the three-dimensional heart structure (189).

The emergence of 3D in vitro models to overcome the limitations of 2D has been under development for many years and they show growing potential as disease models and treatment platforms. One of the most common methods to develop a 3D culture is the production of a cell-loaded hydrogel. A hydrogel is defined as an insoluble, cross-linked polymer network that is able to retain a large amount of water and biological fluids in their swollen states (180). This approach facilitates the cells to live in a three-dimensional matrix. This allows cells to grow at different levels according to the size and depth of the hydrogel (191). Moreover, hydrogel models for cardiac ablation studies can provide additional information about the depth of ablation, an important parameter in vivo that cannot be determined in a 2D cell model.

Tissue conductivity is a physical property that measures the ease at which electric charge can pass through a material (in this case a tissue). It has been reported to conductivity can have a significant effect on cell death and permeabilization. In suspension cultures and monolayer cell ablation studies, this value is determined by the extracellular solution used in the ablation process (192). In hydrogel experiments, this value is given by the composition of the hydrogel and will ultimately affect the ablation size.

Hyaluronic acid (HA) is a naturally occurring linear unbranched polysaccharide (glycosaminoglycan) and one of the primary components of the extracellular matrix (ECM). HA is used for tissue engineering due to its inherent biocompatibility, biodegradability and viscoelastic characteristics (193). HA chemical structure allows the addition of other chemical compounds to modify and improve its properties as a hydrogel scaffold (194). In addition to HA, collagen is an alternative component used in 3D culture systems. Collagen is the main natural protein of connective tissues (skin, bones, tendon, basal membranes) and has an essential role in maintaining structural integrity for tissues (195). The use of collagen hydrogels as a substrate for cell culture improves cell growth, differentiation and adherence for many cell types (196,197).

Choosing a correct model composition that improves cell viability, mimics the electrical conductivity found in native tissues and can be used for ablation studies is a significant challenge. This study aims to develop and optimise a three-

dimensional cardiac model to use as a platform for catheter ablation testing. To this aim, this chapter emphasises the optimization process of model of higher complexity compared to those of Chapter 2. In this chapter, processes such as the fabrication procedure, analysis of hydrogel conductivity, study of cell viability and morphology and the effect of ablation parameters are described for two hydrogel candidates.

2. Materials and Methods

Cell culture

Human cardiomyocyte cells AC16 (Sigma-Aldrich) were cultured in T75 flasks and passaged with trypsin-EDTA 0.025% (Sigma-Aldrich) every 2-3 days for maintenance. Cardiomyocytes were cultured in Dulbecco's Modified Eagle's Medium/Ham's Nutrient Mixture F-12 (DMEM/F-12) (Sigma Aldrich) supplemented with 12.5% Foetal bovine serum (FBS) (Gibco), 1% Penicillin/Streptomycin (Sigma Aldrich) and 2 mM L-Glutamine (Sigma Aldrich). For adherent cell experiments, 6 well plates were coated with 0.1 mg/ml gelatin before cardiomyocytes were seeded with a cell density of 7.5×10^5 cells per well overnight to ensure complete confluence.

Hyaluronic acid gel fabrication

A 1.5% (w/v) HA gel preparation was made using lyophilised HA added to phosphate buffer saline (PBS, Sigma Aldrich) at a concentration of 15 mg/mL and rehydrated overnight on a rotational rocker at 4°C. The polymer solution was subsequently divided into two equal volumes and horseradish peroxidase (HRP) was added to one solution together with the cells while 0.1% hydrogen peroxide (H₂O₂) was added to the other solution. Equal volumes (30 µl for each ml of solution) of the HRP and H₂O₂ polymer solutions were drawn into separate Luer lock syringes before being expelled synchronously through a plastic mixer. Hydrogels were injected into custom-made plastic ring scaffolds placed inside of a 6-well plate, where the resulting hydrogels were 24 mm diameter, 2 mm height and 1.2 ml volume. Similarly, 24 well plates were used as scaffolds for viability experiments using a total of 400 µl of total volume. The gel forms almost instantly, and culture

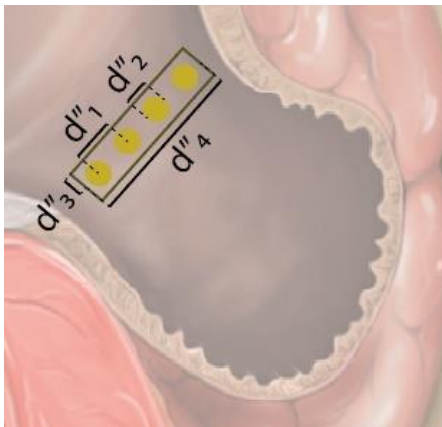
media was added until complete coverage of the gel was achieved. The final concentration of cells in each gel was 2 million/gel.

Collagen I gel fabrication

A 1.5 mg/ml collagen I from rat tail solution (IBIDI) was prepared following the manufacturer's instructions. In summary, the collagen I solution was diluted using 10X DMEM, ddH₂O and neutralised using NaOH and NaHCO₃. A cell suspension containing one million cells was added in culture media and mixed homogeneously before adding the mix to 12 or 24 well plates (1 ml and 400 μ l of total volume respectively), which act as scaffolds. The gel mixture was placed in the incubator for 30 minutes for polymerization and culture media was added until complete coverage of the gel was achieved.

Conductivity measurement of the hydrogels

To assess the conductivity of the hydrogel, a collinear probe was utilised. The electrodes of the probe were chosen with a radius larger than 1 mm, as a radius larger than 1 mm has been shown to reduce non-linearities, electrode impedance and electrode polarization. Therefore, the total footprint of the proposed probe is 20 mm by 4 mm. The collinear probe is shown in Figure 3.1B, and a schematic representation overlaid on the LAA in Figure 3.1A, where the dimensions are $d''_1 = 5$ mm, $d''_2 = 3$ mm, $d''_3 = 2$ mm, $d''_4 = 20$ mm.



(a) (b)

Figure 3. 1. Conductivity measurement probe. (a) Diagram showing the dimensions of the proposed collinear probe with small electrodes. The illustration shows the footprint of the probe on the surface of the LAA, (b) Photo of the manufactured prototype of the proposed collinear probe with small electrodes.

The acquisition of the conductivity passed from acquiring the frequency-dependent complex impedance and was performed using the methods described in (198) using a PGSTAT204 (Autolab, Kanaalweg The Hague, The Netherlands) in galvanostat mode at room temperature with Nova 2.1 software. The galvanostatic mode was used with a 100 μ A flowing between the inducing electrodes. The measurement setup consists of the PGSTAT204 connected to the proposed probe (i.e., working electrode, counter electrode, reference electrode and sensing electrode) and the PGSTAT204 connected to a computer that uses the Nova 2.1 to control the PGSTAT204. The probe was designed to fit into a holder that is attached to a retort stand to maintain the stability of the set up. The full set up used is shown in Figure 3.2 below.

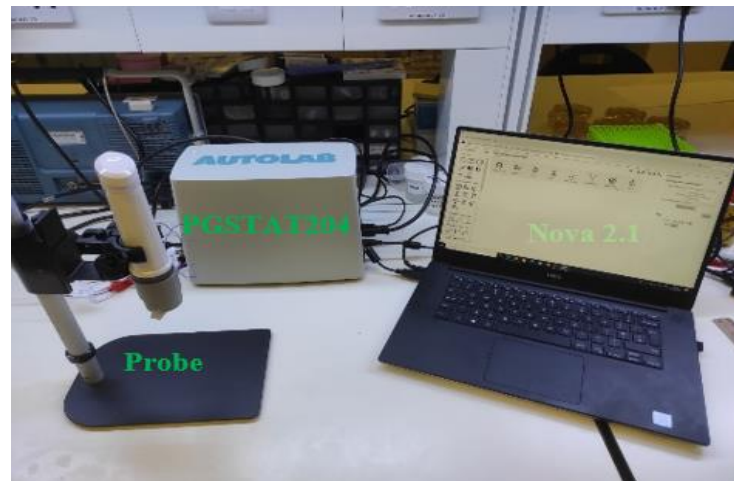


Figure 3. 2. Measurement setup with the probe, the laptop running NOVA 2.1 software in the foreground. PGSTAT204 potentiostat/galvanostat and the probe holder used to lift and keep the probe fixed.

The first step of computing the conductivity is determining the cell constant (k), k is the factor that relates measured conductance and the corresponding reference conductivity. The k for the proposed collinear probe is 0.032 m for the collinear probe for the frequency range from 0.1 Hz to 100 kHz (with the Pearson correlation

coefficient R between the measured conductance and the reference conductivity 0.99 for the collinear probe). The second step is calculating the electrical conductivity from the measured impedance data and the cell constant using equation 1 (199).

$$k=G/\sigma \quad \text{(Equation 1)}$$

where σ is the electrical conductivity of the standard liquids and G is the measured conductance of the probe in the targeted frequency range. In theory, the 0.3% NaCl solution is chosen to determine k as there are no dielectric dispersions in ionic aqueous solutions at frequencies below 1 MHz (200). Therefore, the measured complex impedance is frequency independent and only varies with the concentrations of the aqueous NaCl solution (201).

Cell Counting assay

Cardiomyocyte cells were counted and seeded at the desired cell density in HA or collagen I hydrogels in 12 well culture plates (Corning). After incubation at 37 °C in a humidified atmosphere with 5% CO₂ for 24, 48 and 72 h, 10% of the total media volume of Cell counting assay (CCK-8) reagent (Sigma Aldrich) was added into each well and absorbance at 450 nm read using a microplate reader (Hidex).

Ablation parameter screening in a monolayer model

Cardiomyocyte cells were counted and seeded at a cell density of 7.5×10^5 cells per well in gelatin-coated 6-well plates to ensure complete confluence. After incubation at 37 °C in a humidified atmosphere with 5% CO₂ for 24h, media was removed and substituted by PBS and cultures ablated in the culture well plate using a custom-printed probe for ablation (Figure 3.3 A) with electrode size 3x5 mm and centre-centre gap of 8 mm. The electrodes were connected to a biphasic wave generator placed and they were placed 1 mm above the cell layer. Cells were ablated applying a total of 15,000 pulses of 2 μ s pulse duration (Total on-time of 60ms). The initial range tested was 0-1000 V, however the highest voltage produced sparking on the electrodes and was not used for further testing.

Hydrogel ablation

After incubation at 37 °C in a humidified atmosphere with 5% CO₂ for 24h, media was removed from the hydrogels and custom-printed probes (Figure 3.3 B,C) were connected to a biphasic wave generator and placed in contact with the hydrogel surface. Parameters used were the same as the ones used for the screening model, with the selected input voltage of 750 V. Two different electrode spacings were used, 8 mm and 10 mm centre-centre.

Live-Dead assay

The ablation area in samples was assessed by incubation with 3 µM PI and 1.5 µM Calcein-AM (30 minutes, 37°C) (Sigma-Aldrich) and images were obtained by scanning the wells using EVOS M7000 Imaging System and Olympus Fluoview 3000 Confocal Microscope. Images were analysed using NIH ImageJ to determine the ablation area.

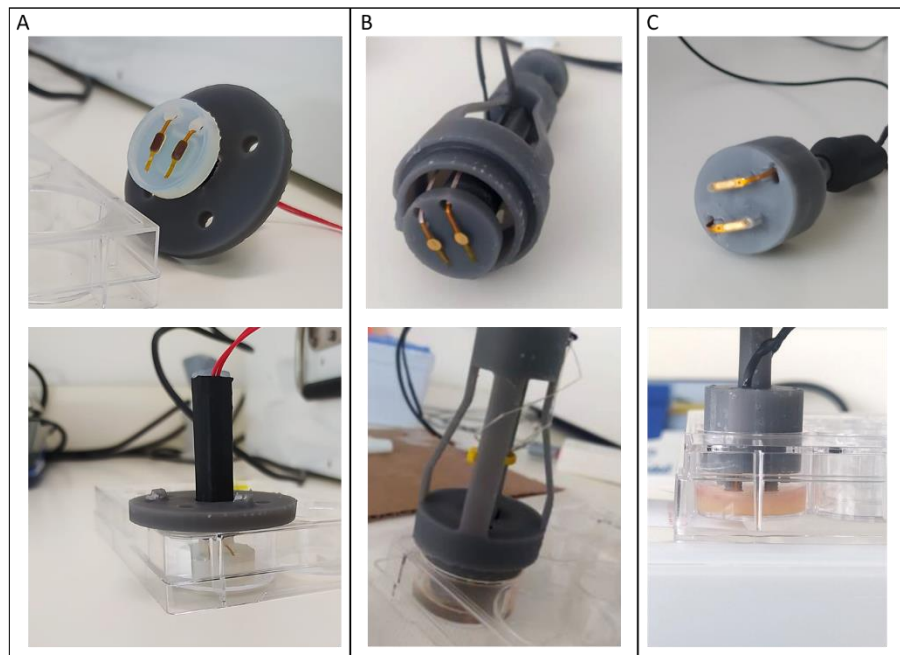


Figure 3.3. Custom-printed electrodes and ablation set ups for (A) monolayer ablation (B) HA hydrogel ablation (C) Collagen I hydrogel ablation.

Statistical analysis

Data were analysed using one-way and two-way ANOVA and multiple comparison tests using GraphPad 9.0. Experiments were repeated for at least three independent experimental blocks with three technical replicates (N=9). Statistical analyses were performed with a confidence level of $\alpha = 0.05$.

3. Results and Discussion

Hyaluronic Acid vs Collagen I hydrogels – Cell viability

The appropriate hydrogel model for in vitro cardiac ablation must allow the proliferation and growth of viable cells. To this aim, increasing AC16 cell densities were seeded into HA and Collagen I hydrogels and the viability was measured using the CCK-8 assay at three different time points (24, 48 and 72 hours post-seeding) (Figure 3.4). All experiments were performed in 24 well plates with the plate walls acting as a mould for the hydrogels.

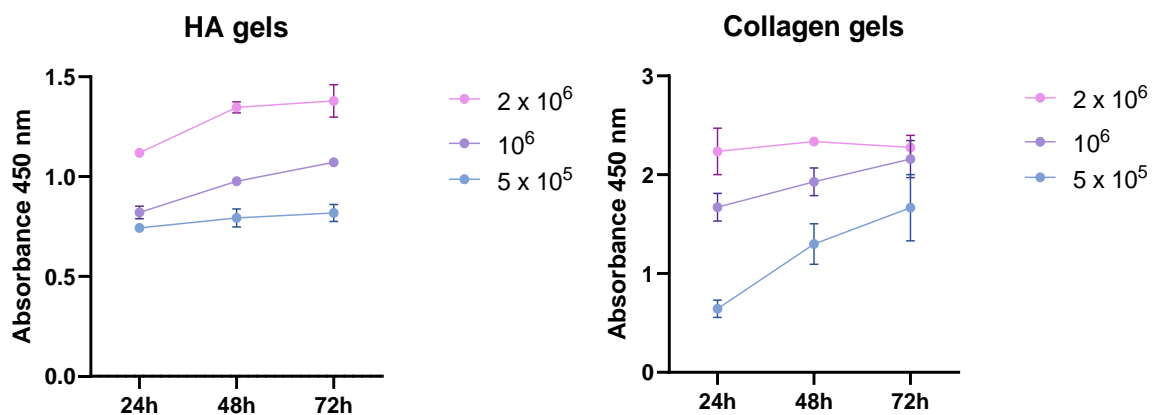


Figure 3. 4. Growth curves of increasing densities of AC16 cells in HA and Collagen I hydrogels. Higher values of absorbance are proportional to a higher number of viable cells.

Table 3.1. Two-way ANOVA table for repeated measures. Data is representative of at least 3 independent experiments (**P < 0.05).

Source of Variation	P value	P value summary
Row Factor x Column Factor	0.0740	ns
Row Factor	0.0039	**
Column Factor	0.0044	**
Subject	0.0691	ns

A two-way ANOVA for repeated measures was performed to analyse the effect of cell density and time on HA versus collagen cell viability. It revealed that there was not a statistically significant interaction between the effects of cell density and time ($p = 0.0740$). Simple main effects analysis showed that both cell density and time have a statistically significant effect on HA versus collagen cell viability individually ($p = 0.0044$ and $p = 0.0039$ respectively).

Collagen I gels support an overall higher AC16 viability in culture, showing a higher proliferation capacity for lower cell densities compared to higher cell density, where it remains stable over time. A different scenario is found in HA gels, where the higher cell density shows a higher proliferation capacity while the lowest density maintains a low proliferation rate. Growth curves were used to select the optimal cell density for further experiments. In the design of the ablation experiments cells are not required to be in hydrogel culture for more than 24-30h, a high number of cells can be adequate. For HA gels, 2×10^6 cells/gel was chosen to maintain a proliferative profile which indicates a healthy culture and the values at 24h were significantly higher than lower cell densities. For Collagen I gels, 1×10^6 cells/gel was chosen as cells at this density still have proliferation capacity and the viability was significantly higher than 5×10^5 cells/gel.

Hydrogels seeded with the chosen cell density were imaged to visualise cell morphology in the hydrogel. The hydrogels were stained using Live/Dead fluorescent staining and whole hydrogel images were taken using the fluorescent microscope EVOS M7000 microscope system (Thermo Fisher Scientific) (Figure 3.5).

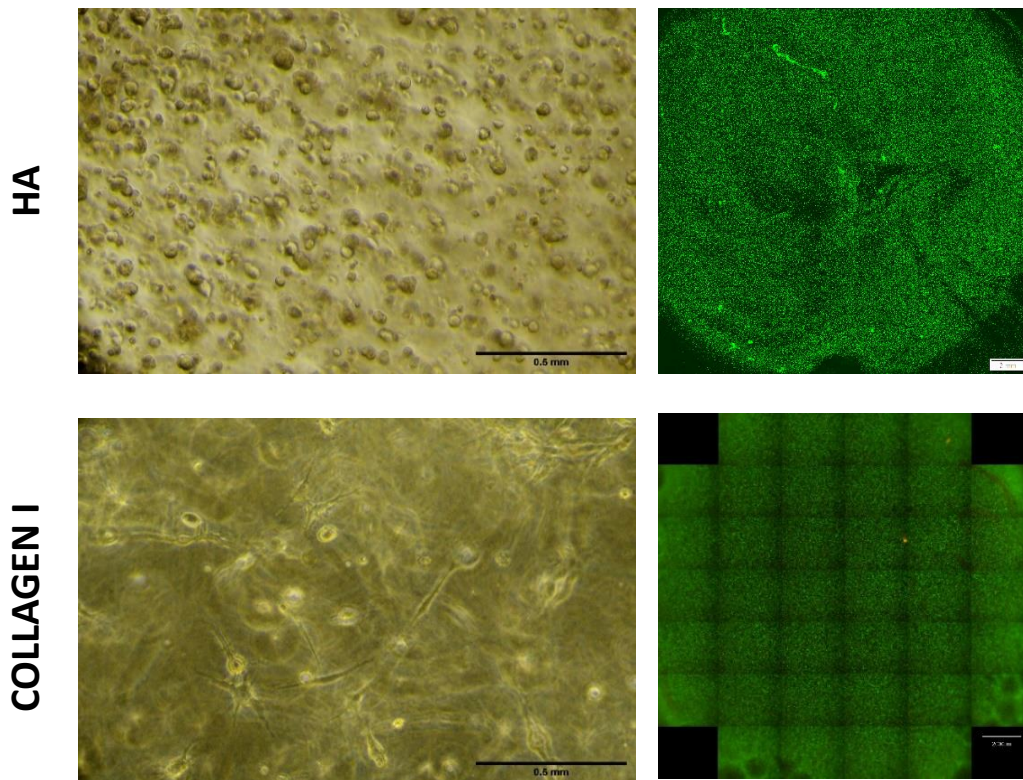


Figure 3. 5.Light microscope imaging and Live/Dead staining of AC16 cells in HA and Collagen I hydrogel cultures after 24h in culture. The images show the cell morphology in the hydrogels and the cell viability labelling cells with green dye (Calcein-AM). The scale bar in fluorescent images corresponds to 2 mm.

HA and collagen I hydrogels have different effects on cell morphology. HA gel promotes the aggregation of cells and the formation of spheroids, confirmed by the presence of several nuclei in the spheroids (Figure 3.6). Collagen I allows the cells to stretch and form a more typical cardiomyocyte elongated morphology, similar to the shape seen in monolayer cultures. In both cases, cells were viable all over the hydrogel and the number of dead cells was minimal. This confirms that HA and Collagen I hydrogels are appropriate to create a homogeneous and viable cell culture over time.

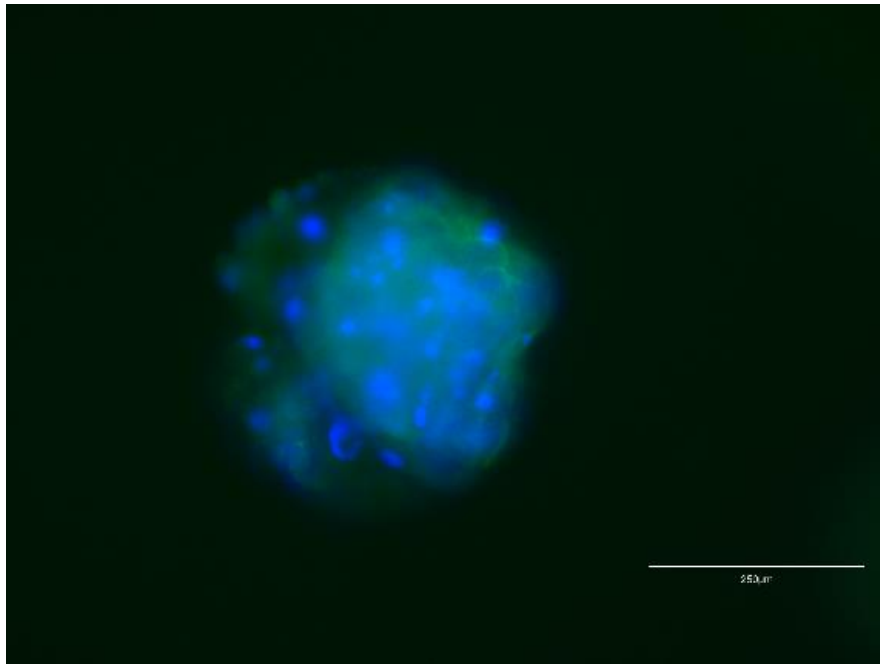


Figure 3.6. Cells spheroid in HA hydrogel culture stained with phalloidin for the cytoskeleton (green) and DAPI for nuclei (blue). The image reveals the presence of several nuclei and therefore cells in each spheroid. Scale bar = 250 μm .

Hyaluronic Acid vs Collagen I hydrogels – Hydrogel conductivity

Given the importance of the conductivity of the hydrogel in the ablation process, conductivity values of the hydrogels were measured and compared with in vivo and ex vivo tissue conductivity of the Left atrial appendage (LAA), as well as blood.

Measurements of electrical conductivity of the hydrogels were performed with a 4-electrode probe method. The measured complex electrical impedance was used to calculate the electrical conductivity of the normal hydrogel, hydrogel with 20 mM sucrose, hydrogel with collagen, blood, LAA both ex vivo and in vivo. To further validate the measurement set up, three pre- and post-validation measurements with 0.15M NaCl solution and were acquired to show any drift in the measurement.

The results from all the conductivity measurements were compared. The conductivity the normal hydrogel, hydrogel with 20 mM sucrose, hydrogel with collagen, blood, LAA ex vivo and in vivo displays a wide range from 0.2 S/m to

1.5 S/m. The variation of the conductivity of the normal hydrogel and the hydrogel with sucrose is observed to be double the conductivity of the hydrogel with collagen. Additionally, the hydrogel with collagen is observed to display a conductivity similar to the range of LAA, and blood.

Furthermore, the drift from the pre- and post-validation measurement show a characteristic zero drift and sensitivity drift that averages at 2.5%.

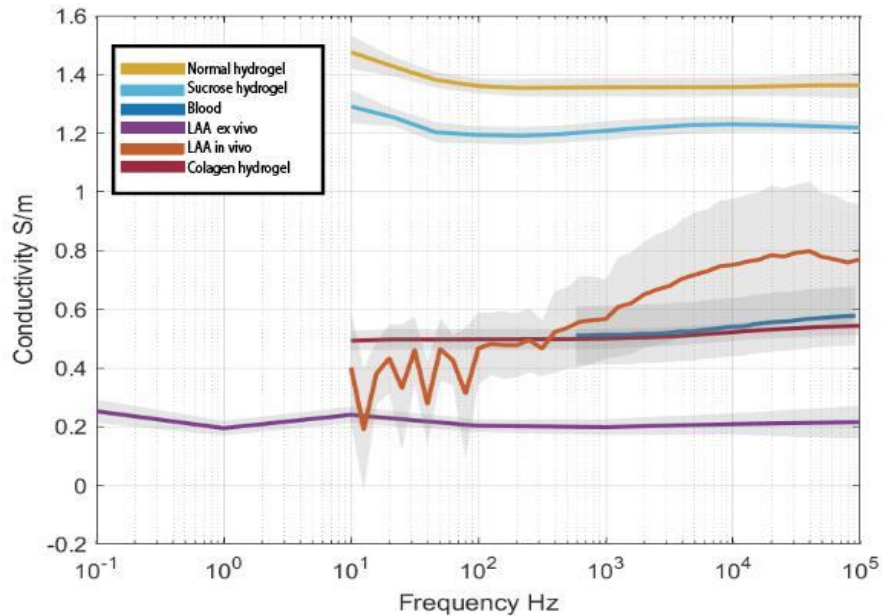


Figure 3.7. Conductivity measurements acquired from the normal hydrogel, hydrogel with 20 mM sucrose, hydrogel with collagen, blood, LAA ex vivo and in vivo.

As shown in the Figure 3.7, HA conductivity was far from left atrial appendage and blood values. This led to test the effect of addition of 20 mM sucrose (a big, apolar molecule well tolerated by cells) in order to reduce the conductivity value. This sucrose concentration was added in the PBS used to rehydrate the HA. The sucrose HA hydrogel had a lower conductivity but was not close enough to the optimal values. Collagen I hydrogels, on the other hand, had a closer conductivity to blood and LAA measurements, indicating it would be a better candidate for the ablation testing.

Ablation voltage screening

Input voltage is one of the parameters that has been shown to have a greater effect on ablation, therefore the selection of an appropriate voltage is essential to create a controlled ablation area. Prior to testing ablation on the hydrogel set-up, increasing voltages were tested in a AC16 monolayer model to select a value that would create a measurable ablation. The results of this preliminary experiment are shown in Figure 3.8.

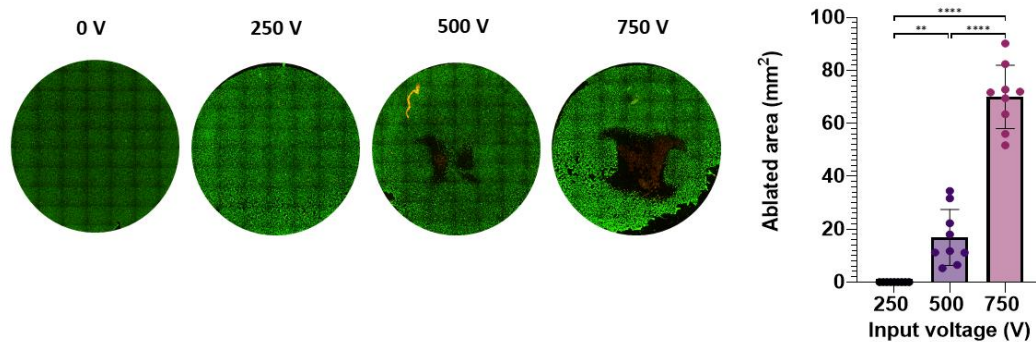


Figure 3.8. Cardiomyocyte ablated area produced by increasing input voltages. Ablations were performed using the probe used in monolayer experiments, keeping the other ablation parameters constant (table). Data is representative of at least 3 independent experiments. Data were analysed with one-Way ANOVA and Multiple comparisons test. **P < 0.05, ****P < 0.0001.

Inside of the final range of 0-750 V, no ablation was detected applying 0 or 250 V, while increasing the voltage to 500 V led to the formation of an ablation zone, which was small in most cases. 750 V produced significantly bigger ablation areas, leading to the selection of this value as input voltage for the ablation test.

Ablation test – Collagen I hydrogels

Collagen I hydrogel had the best viability and conductivity characteristics and thus was used for ablation testing. A 3D-printed probe was designed for the ablation, and the set up was prepared as indicated in Figure 3.3B.

After applying the pulse parameters selected in Table 3.1 and the input voltage of 750 V, the collagen hydrogel structure did not survive the ablation, and the remaining components became liquid in the well. Reducing the input voltage to 500 V reduced the gel breakdown (Figure 3.9), but it was not possible to perform any assessment of the ablated area.



Figure 3.9. Broken collagen I hydrogels after ablation. Left hydrogel was treated with 750V and right hydrogel was treated with 500 V.

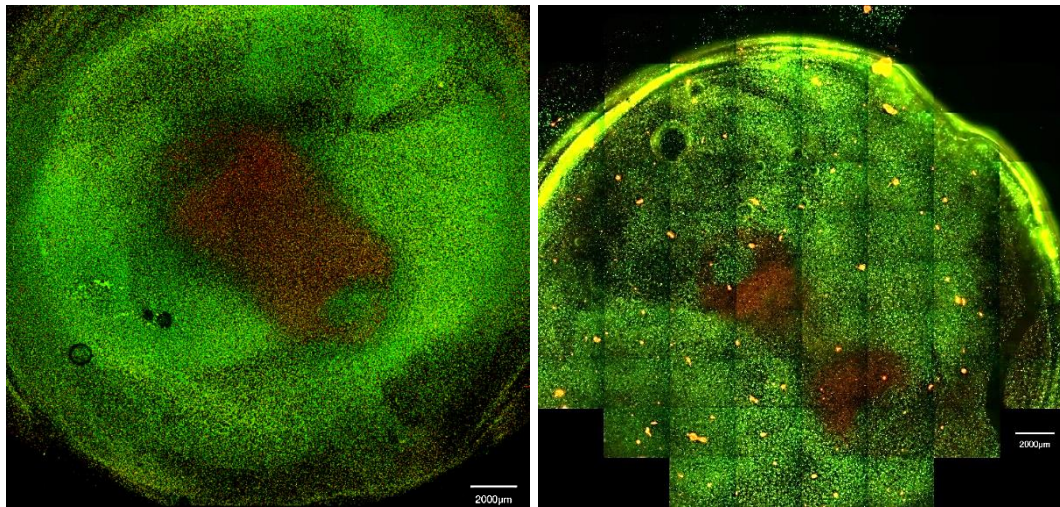
The conclusion of these results was that collagen I hydrogel structure was not suitable for ablation experiments, showing potential as a cardiac model but not as an ablation model. Some possible reasons behind this phenomenon have been previously reported, and appear to be related to increases in temperature during ablation (melting of the collagen hydrogels, which occurs at approximately 43–45°C (202)) or the use of higher collagen concentrations that are not available in commercial stocks (139). Previous studies in collagen I ablations use pin electrodes compared to the planar electrodes used in this experiment, suggesting that electrode design has an important effect on the hydrogel reaction to ablation, and may be an area of future investigation (203).

Ablation test – HA hydrogels ablation

HA hydrogels were ablated without disruption of their structure. Large hydrogels were made, and 3D printed probe were made for them. The set up was prepared as indicated in Figure 3.1.

The structure of the hydrogel was not negatively affected by the pulse delivery, and the hydrogels maintained their structure which allowed further assessment of the ablation zone. At 2h post ablation, the hydrogels were stained using Live/Dead staining to determine live and dead cell areas in the hydrogel. Using two different electrode spacings were tested, 8 mm and 10 mm centre to

centre. At 2 h post-ablation, fluorescent images were acquired, and ablation areas were subsequently measured (Figure 3.10).



Electrode spacing	Ablated area (mm ²)
8 mm	63.47 ± 3.89
10 mm	55.01 ± 1.73

Figure 3.10. Ablation zones created in HA hydrogel model after pulse delivery using 8mm and 10 mm c-c electrode probes. Dead cells are stained in red (PI) and live cells in green (Calcein AM).

The ablation imaging results clearly show the ablated area produced by the input pulse parameters in two different electrode spacing probes. Increasing the electrode spacing creates longer ablations but smaller ablated areas that are slightly connected compared to the bigger middle ablation in 8 mm spacing- treated samples. Previous studies have highlighted the effect of the input ablation parameters on the ablated area such as voltage (204) or number of pulses (140). These results highlight the effect of electrode design on the ablated zone, indicating the potential of this model to test not only input parameters but also electrode prototypes.

4. Conclusions

The selection of an appropriate in vitro model that can be appropriately used for initial preclinical testing is a difficult decision. Contrary to drug screenings, ablation screenings include the additional challenge of the electric and physical effects of applying electric pulses through specific electrode designs. Therefore, the use of tri-dimensional models is needed to allow the contact of the electrodes directly with the matrix where the cells are embedded. Providing an appropriate environment for cell growth and distribution, together with an adequate conductivity similar to the target tissue are essential variables to take into account when designing a tri-dimensional in vitro model.

This work has shown the selection process between two hydrogels in vitro models for cardiac ablation. The results highlight the importance of designing a model according to the purpose of it. An improved cardiac in vitro model such as collagen I hydrogel can have potential benefits in disease modelling or drug testing, but it is not a suitable model for cardiac ablation as it is not able to bear the application of electric pulses. HA hydrogels have shown the robustness needed for ablation testing, allowing the ablation of cardiomyocytes without disrupting the hydrogel structure. Moreover, the HA hydrogel can be easily stained and imaged to measure the ablation area. This proposed model has plenty of opportunities for improvement regarding cell morphology and conductivity, but it provides a good starting point to develop better models for in vitro cardiac ablation.

Chapter 4 – Conclusions

This project explored the importance of using an optimised model for the preclinical testing of a specific therapeutic for Afib. Three different models (cell suspension, cell monolayer and hydrogel) with different levels of complexity have been analysed and used as ablation models to treat Afib. Each model has provided specific information that has helped the design and parameter selection for models with higher complexity.

The suspension cardiomyocyte model has shown potential as an initial testing platform due to the large amount of data that can be obtained from it, making it an attractive model for screening studies of broad-range parameters. In this study, this model helped to analyse the effect of field strength, pulse width and burst number on cardiomyocyte cell death and the interaction between these parameters. The data highlights the importance of the on-time on the electroporation process and the major impact of the pulse duration on cell death but also the negative side effects of very long pulses.

The 2D ablation model using a monolayer of cardiomyocytes provides the advantage of visualising the ablation area created by selected pulse parameters, and the evolution of the lesion over time. The results of this model show the time dependence of cell death using IRE, obtaining bigger lesions 24h post-ablation than at earlier time points, suggesting the activation of delayed cell death pathways such as apoptosis. These findings are important to consider when selecting the assessment time of ablation treatment, as it can change over time. These models provide useful information but also present limitations regarding the absence of tri-dimensional structure and accurate conductivity measurements, a key component in the ablation process.

To overcome these limitations, two potential 3D hydrogel models were designed. The results obtained through the optimization process indicated the importance of selecting an appropriate hydrogel that maintains cell viability and resists the pulse application process. Two common hydrogels (hyaluronic acid and collagen I) were chosen as candidates. Despite collagen I show promising results in creating an appropriate cell culture environment for cell growth and a similar

conductivity as cardiac tissue, it was not able to maintain stability after pulse application. HA hydrogel, on the other hand, showed good resistance to ablation treatment and allowed the staining and imaging of the ablation area post-ablation.

Overall, this project highlights the potential use of IRE to achieve effective ablations for the clinical treatment of Afib and gives new insights into the effect of IRE on cell death. In addition, it shows the design of an ablation tri-dimensional model which can be applied to any cell type and gives a broad range of opportunities to explore not only pulse parameters but also different electrode geometry and designs.

Bibliography

1. Staerk L, Sherer JA, Ko D, Benjamin EJ, Helm RH. Atrial fibrillation: epidemiology, pathophysiology, and clinical outcomes. *Circ Res.* 2017 Apr 28;120(9):1501–1517.
2. Krijthe BP, Kunst A, Benjamin EJ, Lip GYH, Franco OH, Hofman A, *et al.* Projections on the number of individuals with atrial fibrillation in the European Union, from 2000 to 2060. *Eur Heart J.* 2013 Sep;34(35):2746–2751.
3. Morin DP, Bernard ML, Madias C, Rogers PA, Thihalolipavan S, Estes NAM. The state of the art: atrial fibrillation epidemiology, prevention, and treatment. *Mayo Clin Proc.* 2016 Dec;91(12):1778–1810.
4. Gawalko M, Kapłon-Cieślicka A, Hohl M, Dobrev D, Linz D. COVID-19 associated atrial fibrillation: Incidence, putative mechanisms and potential clinical implications. *Int J Cardiol Heart Vasc.* 2020 Oct;30:100631.
5. January CT, Wann LS, Alpert JS, Calkins H, Cigarroa JE, Cleveland JC, *et al.* 2014 AHA/ACC/HRS guideline for the management of patients with atrial fibrillation: a report of the American College of Cardiology/American Heart Association Task Force on Practice Guidelines and the Heart Rhythm Society. *J Am Coll Cardiol.* 2014 Dec 2;64(21):e1–76.
6. Haïssaguerre M, Jaïs P, Shah DC, Takahashi A, Hocini M, Quiniou G, *et al.* Spontaneous initiation of atrial fibrillation by ectopic beats originating in the pulmonary veins. *N Engl J Med.* 1998 Sep 3;339(10):659–666.
7. Wu TJ, Liang KW, Ting CT. Relation between the rapid focal activation in the pulmonary vein and the maintenance of paroxysmal atrial fibrillation. *Pacing Clin Electrophysiol.* 2001 May;24(5):902–905.
8. Sanders P, Morton JB, Davidson NC, Spence SJ, Vohra JK, Sparks PB, *et al.* Electrical remodeling of the atria in congestive heart failure: electrophysiological and electroanatomic mapping in humans. *Circulation.* 2003 Sep 23;108(12):1461–1468.
9. Mahida S, Sacher F, Derval N, Berte B, Yamashita S, Hooks D, *et al.* Science linking pulmonary veins and atrial fibrillation. *Arrhythm Electrophysiol Rev.* 2015 May 30;4(1):40–43.

10. Azevedo PS, Polegato BF, Minicucci MF, Paiva SAR, Zornoff LAM. Cardiac remodeling: concepts, clinical impact, pathophysiological mechanisms and pharmacologic treatment. *Arq Bras Cardiol.* 2016 Jan;106(1):62–69.
11. Sanfilippo AJ, Abascal VM, Sheehan M, Oertel LB, Harrigan P, Hughes RA, *et al.* Atrial enlargement as a consequence of atrial fibrillation. A prospective echocardiographic study. *Circulation.* 1990 Sep;82(3):792–797.
12. Heijman J, Voigt N, Nattel S, Dobrev D. Cellular and molecular electrophysiology of atrial fibrillation initiation, maintenance, and progression. *Circ Res.* 2014 Apr 25;114(9):1483–1499.
13. Veenhuyzen GD. Atrial fibrillation/George D. Veenhuyzen, Christopher S. Simpson, A. Hoshiar. *CMAJ.* 2004;171:7.
14. Lafuente-Lafuente C, Valembois L, Bergmann J-F, Belmin J. Antiarrhythmics for maintaining sinus rhythm after cardioversion of atrial fibrillation. *Cochrane Database Syst Rev.* 2015 Mar 28;(3):CD005049.
15. Vw Em. A classification of antiarrhythmic actions reassessed after a decade of new drugs. *J Clin Pharmacol.* 1984;
16. Zimetbaum P. Antiarrhythmic drug therapy for atrial fibrillation. *Circulation.* 2012 Jan 17;125(2):381–389.
17. Roden DM. Risks and benefits of antiarrhythmic therapy. *N Engl J Med.* 1994 Sep 22;331(12):785–791.
18. Ecker V, Knoery C, Rushworth G, Rudd I, Ortner A, Begley D, *et al.* A review of factors associated with maintenance of sinus rhythm after elective electrical cardioversion for atrial fibrillation. *Clin Cardiol.* 2018 Jun 7;41(6):862–870.
19. Calkins H. Heart Rhythm Society Task Force on Catheter and Surgical Ablation of Atrial Fibrillation. *Heart Rhythm.* 2012; 9 :632-696
20. Calkins H, Reynolds MR, Spector P, Sondhi M, Xu Y, Martin A, *et al.* Treatment of atrial fibrillation with antiarrhythmic drugs or radiofrequency ablation: two systematic literature reviews and meta-analyses. *Circ Arrhythm Electrophysiol.* 2009 Aug;2(4):349–361.
21. Di Biase L, Burkhardt JD, Mohanty P, Sanchez J, Mohanty S, Horton R, *et al.* Left atrial appendage: an underrecognized trigger site of atrial fibrillation. *Circulation.* 2010 Jul 13;122(2):109–118.

22. Haegeli LM, Calkins H. Catheter ablation of atrial fibrillation: an update. *Eur Heart J*. 2014 Sep 21;35(36):2454–2459.
23. He DS, Zimmer JE, Hynynen K, Marcus FI, Caruso AC, Lampe LF, *et al*. Application of ultrasound energy for intracardiac ablation of arrhythmias. *Eur Heart J*. 1995 Jul 1;16(7):961–966.
24. Engel DJ, Muratore R, Hirata K, Otsuka R. Myocardial lesion formation using high-intensity focused ultrasound. *Journal of the American Society of Echocardiography*, 2006;19(7):932-937.
25. Schmidt B, Antz M, Ernst S, Ouyang F, Falk P, Chun JKR, *et al*. Pulmonary vein isolation by high-intensity focused ultrasound: first-in-man study with a steerable balloon catheter. *Heart Rhythm*. 2007 May;4(5):575–584.
26. Jin ES, Wang PJ. Cryoballoon ablation for atrial fibrillation: a comprehensive review and practice guide. *Korean Circ J*. 2018;
27. Whittaker DK. Mechanisms of tissue destruction following cryosurgery. *Ann R Coll Surg Engl*. 1984 Sep;66(5):313–318.
28. Kaszala K, Ellenbogen KA. Biophysics of the second-generation cryoballoon: cryobiology of the big freeze. *Circ Arrhythm Electrophysiol*. 2015 Feb;8(1):15–17.
29. Nuccitelli R. Application of pulsed electric fields to cancer therapy. *Bioelectricity*. 2018 Oct;1(1):24–28.
30. Heijman J, Guichard J-B, Dobrev D, Nattel S. Translational challenges in atrial fibrillation. *Circ Res*. 2018 Mar 2;122(5):752–773.
31. Heijman J, Algalarrondo V, Voigt N, Melka J, Wehrens XHT, Dobrev D, *et al*. The value of basic research insights into atrial fibrillation mechanisms as a guide to therapeutic innovation: a critical analysis. *Cardiovasc Res*. 2016 Apr 1;109(4):467–479.
32. Pappone C, Santinelli V, Manguso F, Vicedomini G, Gugliotta F, Augello G, *et al*. Pulmonary vein denervation enhances long-term benefit after circumferential ablation for paroxysmal atrial fibrillation. *Circulation*. 2004 Jan 27;109(3):327–334.
33. Schüttler D, Bapat A, Käab S, Lee K, Tomsits P, Clauss S, *et al*. Animal models of atrial fibrillation. *Circ Res*. 2020 Jun 19;127(1):91–110.

34. Verheule S, Sato T, T Everett IV, Engle SK. Increased vulnerability to atrial fibrillation in transgenic mice with selective atrial fibrosis caused by overexpression of TGF- β 1. *Circulation research*, 2004; 94(11):1458-1465
35. Zhang M, Hill MC, Kadow ZA, Suh JH, Tucker NR, Hall AW, *et al.* Long-range Pitx2c enhancer-promoter interactions prevent predisposition to atrial fibrillation. *Proc Natl Acad Sci USA*. 2019 Oct 21;
36. Charpentier F, Demolombe S, Escande D. Cardiac channelopathies: from men to mice. *Ann Med*. 2004 Jan 1;36 Suppl 1:28–34.
37. Kirchhoff JE, Skarsfeldt MA, Muthukumarasamy KM, Simó-Vicens R, Bomholtz SH, Abildgaard L, *et al.* The kca2 channel inhibitor AP14145, but not dofetilide or ondansetron, provides functional atrial selectivity in guinea pig hearts. *Front Pharmacol*. 2019 Jun 19;10:668.
38. Clauss S, Bleyer C, Schüttler D, Tomsits P, Renner S, Klymiuk N, *et al.* Animal models of arrhythmia: classic electrophysiology to genetically modified large animals. *Nat Rev Cardiol*. 2019 Mar 20; 16(8), 457-475
39. Fenner MF, Gatta G, Sattler S, Kuiper M, Hesselkilde EM, Adler DMT, *et al.* Inhibition of Small-Conductance Calcium-Activated Potassium Current (IK,Ca) Leads to Differential Atrial Electrophysiological Effects in a Horse Model of Persistent Atrial Fibrillation. *Front Physiol*. 2021 Feb 9;12:614483.
40. Wiedmann F, Beyersdorf C, Zhou X, Büscher A, Kraft M, Nietfeld J, *et al.* Pharmacologic TWIK-Related Acid-Sensitive K⁺ Channel (TASK-1) Potassium Channel Inhibitor A293 Facilitates Acute Cardioversion of Paroxysmal Atrial Fibrillation in a Porcine Large Animal Model. *J Am Heart Assoc*. 2020 May 9;e015751.
41. Frydrychowski P, Michałek M, Sławuta A. Large animals as models of atrial fibrillation. *Advances in Clinical & Experimental Medicine* 2020; 29(6).
42. Westling J, Westling W, Pyle RL. Epidemiology of atrial fibrillation in the dog. *International Journal of Applied Research in Veterinary Medicine*, 2008; 6(3): 151-154
43. Decloedt A, Schwarzwald CC, De Clercq D, Van Der Vekens N, Pardon B, Reef VB, *et al.* Risk factors for recurrence of atrial fibrillation in horses after cardioversion to sinus rhythm. *J Vet Intern Med*. 2015 Jun;29(3):946–953.

44. Nattel S, Liu L, St-Georges D. Effects of the novel antiarrhythmic agent azimilide on experimental atrial fibrillation and atrial electrophysiologic properties. *Cardiovasc Res.* 1998 Mar 1;37(3):627–635.
45. Pritchett ELC, Marcello SR. Azimilide for atrial fibrillation: clinical trial results and implications. *Cardiac Electrophysiology Review.* 2003;
46. Wittkamp FH, van Driel VJ, van Wessel H, Vink A, Hof IE, Gründeman PF, *et al.* Feasibility of electroporation for the creation of pulmonary vein ostial lesions. *J Cardiovasc Electrophysiol.* 2011 Mar;22(3):302–309.
47. Madhavan M, Venkatachalam KL, Swale MJ, Desimone CV, Gard JJ, Johnson SB, *et al.* Novel percutaneous epicardial autonomic modulation in the canine for atrial fibrillation: results of an efficacy and safety study. *Pacing Clin Electrophysiol.* 2016 May;39(5):407–417.
48. van Driel VJHM, Neven K, van Wessel H, Vink A, Doevendans PAFM, Wittkamp FHM. Low vulnerability of the right phrenic nerve to electroporation ablation. *Heart Rhythm.* 2015 Aug;12(8):1838–1844.
49. Du Pré BC, van Driel VJ, van Wessel H, Loh P, Doevendans PA, Goldschmeding R, *et al.* Minimal coronary artery damage by myocardial electroporation ablation. *Europace.* 2013 Jan;15(1):144–149.
50. Koruth JS, Kuroki K, Kawamura I, Brose R, Viswanathan R, Buck ED, *et al.* Pulsed field ablation versus radiofrequency ablation: esophageal injury in a novel porcine model. *Circ Arrhythm Electrophysiol.* 2020 Mar;13(3):e008303.
51. Robbins IM, Colvin EV, Doyle TP, Kemp WE, Loyd JE, McMahon WS, *et al.* Pulmonary vein stenosis after catheter ablation of atrial fibrillation. *Circulation.* 1998 Oct 27;98(17):1769–1775.
52. Nattel S, Dobrev D. Electrophysiological and molecular mechanisms of paroxysmal atrial fibrillation. *Nat Rev Cardiol.* 2016 Aug 4;13(10):575–590.
53. Lau DH, Linz D, Sanders P. New findings in atrial fibrillation mechanisms. *Card Electrophysiol Clin.* 2019;11(4):563–571.
54. Bussek A, Schmidt M, Bauriedl J, Ravens U, Wettwer E, Lohmann H. Cardiac tissue slices with prolonged survival for in vitro drug safety screening. *J Pharmacol Toxicol Methods.* 2012 Sep;66(2):145–151.

55. Rosen MR. Isolated tissue models and proarrhythmia. *European Heart Journal supplements*. 2001; 3(suppl_K), K64-K69
56. Boukens BJ, Sulkin MS, Gloschat CR, Ng FS, Vigmond E, Efimov IR. Transmural APD gradient synchronizes repolarization in the human left ventricular wall. *Cardiovasc Res*. 2015 Jul 24;108(1):188–196.
57. Jost N, Virág L, Comtois P, Ordög B, Szuts V, Seprényi G, *et al*. Ionic mechanisms limiting cardiac repolarization reserve in humans compared to dogs. *J Physiol (Lond)*. 2013 Sep 1;591(17):4189–4206.
58. Gramley F, Lorenzen J, Jedamzik B, Gatter K, Koellensperger E, Munzel T, *et al*. Atrial fibrillation is associated with cardiac hypoxia. *Cardiovasc Pathol*. 2010 Apr;19(2):102–111.
59. Wang R, Yi X, Li X, Jiang X. Fibroblast growth factor-21 is positively associated with atrial fibrosis in atrial fibrillation patients with rheumatic heart disease. *Int J Clin Exp Pathol*. 2015 Nov 1;8(11):14901–14908.
60. Csepe TA, Hansen BJ, Fedorov VV. Atrial fibrillation driver mechanisms: Insight from the isolated human heart. *Trends Cardiovasc Med*. 2017 Jan;27(1):1–11.
61. Page G, Ratchada P, Miron Y, Steiner G, Ghetti A, Miller PE, *et al*. Human ex-vivo action potential model for pro-arrhythmia risk assessment. *J Pharmacol Toxicol Methods*. 2016 Oct;81:183–195.
62. Meyer T, Stuerz K, Guenther E, Edamura M. Cardiac slices as a predictive tool for arrhythmogenic potential of drugs and chemicals. *Expert opinion on drug metabolism & toxicology*, 2010; 6(12):1461-1475.
63. Wettwer E, Christ T, Endig S, Rozmaritsa N, Matschke K, Lynch JJ, *et al*. The new antiarrhythmic drug vernakalant: ex vivo study of human atrial tissue from sinus rhythm and chronic atrial fibrillation. *Cardiovasc Res*. 2013 Apr 1;98(1):145–154.
64. Kang C, Qiao Y, Li G, Baeckle K, Camelliti P, Rentschler S, *et al*. Human organotypic cultured cardiac slices: new platform for high throughput preclinical human trials. *Sci Rep*. 2016 Jun 30;6:28798.
65. Masnok K, Watanabe N. Catheter contact area strongly correlates with lesion area in radiofrequency cardiac ablation: an ex vivo porcine heart study. *Journal of Interventional Cardiac Electrophysiology*, 2021; 1-12

66. Huang S-T, Dong J-Z, Du X, Wu J-H, Yu R-H, Long D-Y, *et al.* Relationship Between Ablation Lesion Size Estimated by Ablation Index and Different Ablation Settings-an Ex Vivo Porcine Heart Study. *J Cardiovasc Transl Res.* 2020 Jun 2; 13, 965-969.
67. Park S, Hwang J, Park JE, Ahn YC. Application of ultrasound thermal imaging for monitoring laser ablation in ex vivo cardiac tissue. *Lasers in surgery and medicine*,2020; 52(3), 218-227
68. Langendorff O. Untersuchungen am überlebenden Säugethierherzen. *Archiv für die gesamte Physiologie des Menschen und der Tiere*, 1895; 61(6); 291-332.
69. Ninio DM, Murphy KJ, Howe PR, Saint DA. Dietary fish oil protects against stretch-induced vulnerability to atrial fibrillation in a rabbit model. *J Cardiovasc Electrophysiol.* 2005 Nov 1;16(11):1189–1194.
70. Sarmast F. Cholinergic atrial fibrillation: IK,ACh gradients determine unequal left/right atrial frequencies and rotor dynamics. *Cardiovasc Res.* 2003 Oct 1;59(4):863–873.
71. Kirchhoff JE, Diness JG, Sheykhzade M, Grunnet M. Synergistic antiarrhythmic effect of combining inhibition of Ca²⁺-activated K⁺ (SK) channels and voltage-gated Na⁺ channels in an isolated heart model of atrial fibrillation. *Heart Rhythm*, 2015;12(2), 409-418.
72. Liao C, Akazawa H, Tamagawa M, Ito K, Yasuda N, Kudo Y, *et al.* Cardiac mast cells cause atrial fibrillation through PDGF-A-mediated fibrosis in pressure-overloaded mouse hearts. *J Clin Invest.* 2010 Jan;120(1):242–253.
73. Chen J, Mandapati R, Berenfeld O, Skanes AC, Gray RA, Jalife J. Dynamics of wavelets and their role in atrial fibrillation in the isolated sheep heart. *Cardiovasc Res.* 2000 Nov;48(2):220–232.
74. Shaffer A, Schinstock E, Bateman M, Iles T, Iaizzo P. Human hearts declined for transplant were resuscitated on the visible heart® apparatus. *J Heart Lung Transplant.* 2019 Apr;38(4):S242.
75. Pak HN, Oh YS, Liu YB, Wu TJ, Karagueuzian HS. Catheter ablation of ventricular fibrillation in rabbit ventricles treated with β -blockers. *Circulation.* 2003; 108(25), 3149-3156.

76. Skrzypiec-Spring M, Grotthus B, Szelag A, Schulz R. Isolated heart perfusion according to Langendorff---still viable in the new millennium. *J Pharmacol Toxicol Methods*. 2007 Apr;55(2):113–126.
77. Doring HJ, Dehnert H. The isolated perfused heart according to Langendorff. BVM-Biomesstechnik Verlag. 1987;
78. Litviňuková M, Talavera-López C, Maatz H, Reichart D, Worth CL, Lindberg EL, *et al*. Cells of the adult human heart. *Nature*. 2020 Dec;588(7838):466–472.
79. Woodcock EA, Matkovich SJ. Cardiomyocytes structure, function and associated pathologies. *Int J Biochem Cell Biol*. 2005 Sep;37(9):1746–1751.
80. Doppler SA, Carvalho C, Lahm H, Deutsch M-A, Dreßen M, Puluca N, *et al*. Cardiac fibroblasts: more than mechanical support. *J Thorac Dis*. 2017 Mar;9(Suppl 1):S36–S51.
81. Simmons MA, Creazzo T, Hartzell HC. A time-dependent and voltage-sensitive K^+ current in single cells from frog atrium. *J Gen Physiol*. 1986 Dec;88(6):739–755.
82. Jahnel U, Nawrath H, Carmeliet E, Vereecke J. Depolarization-induced influx of sodium in response to phenylephrine in rat atrial heart muscle. *J Physiol (Lond)*. 1991 Jan 1;432:621–637.
83. Kuo P-L, Lee H, Bray M-A, Geisse NA, Huang Y-T, Adams WJ, *et al*. Myocyte shape regulates lateral registry of sarcomeres and contractility. *Am J Pathol*. 2012 Dec;181(6):2030–2037.
84. Vites AM, Pappano AJ. Distinct modes of inhibition by ruthenium red and ryanodine of calcium-induced calcium release in avian atrium. *J Pharmacol Exp Ther*. 1994 Mar 1;268(3):1476–1484.
85. Cheung JY, Tillotson DL. Cytosolic free calcium concentration in individual cardiac myocytes in primary culture. *American Journal of Physiology-Cell Physiology*, 1989: 256(6):C1120-C1130
86. Sowell B, Fast VG. Ionic mechanism of shock-induced arrhythmias: role of intracellular calcium. *Heart Rhythm*. 2012 Jan;9(1):96–104.
87. Maqsood MI, Matin MM, Bahrami AR, Ghasroldasht MM. Immortality of cell lines: challenges and advantages of establishment. *Cell Biol Int*. 2013 Oct;37(10):1038–1045.

88. Claycomb WC, Lanson NA, Stallworth BS, Egeland DB, Delcarpio JB, Bahinski A, *et al.* HL-1 cells: a cardiac muscle cell line that contracts and retains phenotypic characteristics of the adult cardiomyocyte. *Proc Natl Acad Sci USA.* 1998 Mar 17;95(6):2979–2984.
89. Ke L, Qi XY, Dijkhuis A-J, Chartier D, Nattel S, Henning RH, *et al.* Calpain mediates cardiac troponin degradation and contractile dysfunction in atrial fibrillation. *J Mol Cell Cardiol.* 2008 Nov;45(5):685–693.
90. Wiersma M, Meijering RAM, Qi X-Y, Zhang D, Liu T, Hoogstra-Berends F, *et al.* Endoplasmic reticulum stress is associated with autophagy and cardiomyocyte remodeling in experimental and human atrial fibrillation. *J Am Heart Assoc.* 2017 Oct 24;6(10).
91. Rao F, Deng C-Y, Wu S-L, Xiao D-Z, Yu X-Y, Kuang S-J, *et al.* Involvement of Src in L-type Ca²⁺ channel depression induced by macrophage migration inhibitory factor in atrial myocytes. *J Mol Cell Cardiol.* 2009 Nov;47(5):586–594.
92. Kimes BW, Brandt BL. Properties of a clonal muscle cell line from rat heart. *Exp Cell Res.* 1976 Mar 15;98(2):367–381.
93. Huang C-Y, Chueh PJ, Tseng C-T, Liu K-Y, Tsai H-Y, Kuo W-W, *et al.* ZAK reprograms atrial natriuretic factor expression and induces hypertrophic growth in H9c2 cardiomyoblast cells. *Biochem Biophys Res Commun.* 2004 Nov 19;324(3):973–980.
94. Vindis C, D'Angelo R, Mucher E, Nègre-Salvayre A, Parini A, Mialet-Perez J. Essential role of TRPC1 channels in cardiomyoblasts hypertrophy mediated by 5-HT_{2A} serotonin receptors. *Biochem Biophys Res Commun.* 2010 Jan 1;391(1):979–983.
95. Davidson MM, Nesti C, Palenzuela L, Walker WF, Hernandez E, Protas L, *et al.* Novel cell lines derived from adult human ventricular cardiomyocytes. *J Mol Cell Cardiol.* 2005 Jul;39(1):133–147.
96. Dutta D, Xu J, Kim J-S, Dunn WA, Leeuwenburgh C. Upregulated autophagy protects cardiomyocytes from oxidative stress-induced toxicity. *Autophagy.* 2013 Mar;9(3):328–344.
97. Cui L, Guo J, Zhang Q, Yin J, Li J, Zhou W, *et al.* Erythropoietin activates SIRT1 to protect human cardiomyocytes against doxorubicin-induced mitochondrial dysfunction and toxicity. *Toxicol Lett.* 2017 Apr 27;275:28–38.

98. Wen J, Shen J, Zhou Y, Zhao X, Dai Z, Jin Y. Pyrroloquinoline quinone attenuates isoproterenol hydrochloride-induced cardiac hypertrophy in AC16 cells by inhibiting the NF- κ B signaling pathway. *Int J Mol Med*. 2020 Jan 10; 45(3), 873-885.
99. Wiegand C, Banerjee I. Recent advances in the applications of iPSC technology. *Curr Opin Biotechnol*. 2019 Dec;60:250–258.
100. Takahashi K, Tanabe K, Ohnuki M, Narita M, Ichisaka T, Tomoda K, *et al*. Induction of pluripotent stem cells from adult human fibroblasts by defined factors. *Cell*. 2007 Nov 30;131(5):861–872.
101. Vogel G. Stem cells. Diseases in a dish take off. *Science*. 2010 Nov 26;330(6008):1172–1173.
102. Burridge PW, Keller G, Gold JD, Wu JC. Production of de novo cardiomyocytes: human pluripotent stem cell differentiation and direct reprogramming. *Cell Stem Cell*. 2012 Jan 6;10(1):16–28.
103. Funakoshi S, Yoshida Y. Recent progress of iPSC technology in cardiac diseases. *Arch Toxicol*. 2021 Dec;95(12):3633–3650.
104. Knollmann BC. Induced pluripotent stem cell-derived cardiomyocytes: boutique science or valuable arrhythmia model? *Circ Res*. 2013 Mar 15;112(6):969–76; discussion 976.
105. Miki Y, Ono K, Hata S, Suzuki T, Kumamoto H, Sasano H. The advantages of co-culture over mono cell culture in simulating in vivo environment. *J Steroid Biochem Mol Biol*. 2012 Sep;131(3-5):68–75.
106. Cartledge JE, Kane C, Dias P, Tesfom M, Clarke L, Mckee B, *et al*. Functional crosstalk between cardiac fibroblasts and adult cardiomyocytes by soluble mediators. *Cardiovasc Res*. 2015 Mar 1;105(3):260–270.
107. Thompson SA, Copeland CR, Reich DH, Tung L. Mechanical coupling between myofibroblasts and cardiomyocytes slows electric conduction in fibrotic cell monolayers. *Circulation*. 2011 May 17;123(19):2083–2093.
108. Rahmutula D, Marcus GM, Wilson EE, Ding C-H, Xiao Y, Paquet AC, *et al*. Molecular basis of selective atrial fibrosis due to overexpression of transforming growth factor- β 1. *Cardiovasc Res*. 2013 Apr 23;

109. Rohr S. Arrhythmogenic implications of fibroblast-myocyte interactions. *Circ Arrhythm Electrophysiol.* 2012 Apr 1;5(2):442–452.
110. Antoni D, Burckel H, Josset E, Noel G. Three-dimensional cell culture: a breakthrough in vivo. *Int J Mol Sci.* 2015 Mar 11;16(3):5517–5527.
111. Tibbitt MW, Anseth KS. Hydrogels as extracellular matrix mimics for 3D cell culture. *Biotechnol Bioeng.* 2009 Jul 1;103(4):655–663.
112. Sirish P, Li N, Timofeyev V, Zhang X-D, Wang L, Yang J, *et al.* Molecular mechanisms and new treatment paradigm for atrial fibrillation. *Circ Arrhythm Electrophysiol.* 2016 May;9(5).
113. Gu J, Liu X, Wang Q-X, Guo M, Liu F, Song Z-P, *et al.* Beneficial effects of pioglitazone on atrial structural and electrical remodeling in vitro cellular models. *J Mol Cell Cardiol.* 2013 Oct 4;
114. Baena-Montes JM, O'Halloran T, Clarke C. Electroporation Parameters for Human Cardiomyocyte Ablation In Vitro. *Journal of Development and Disease,* 2022; 9(8): 240.
115. Théry M. Micropatterning as a tool to decipher cell morphogenesis and functions. *J Cell Sci.* 2010 Dec 15;123(Pt 24):4201–4213.
116. Whitesides GM, Ostuni E, Takayama S, Jiang X, Ingber DE. Soft lithography in biology and biochemistry. *Annu Rev Biomed Eng.* 2001;3:335–373.
117. Xia Y, Whitesides GM. Soft lithography. *Annu Rev Mater Sci.* 1998 Aug;28(1):153–184.
118. Bélisle JM, Kunik D, Costantino S. Rapid multicomponent optical protein patterning. *Lab on a Chip.* 2009; 9(24), 3580-3585.
119. Badie N, Bursac N. Novel micropatterned cardiac cell cultures with realistic ventricular microstructure. *Biophys J.* 2009 May 6;96(9):3873–3885.
120. McDevitt TC, Angello JC, Whitney ML, Reinecke H, Hauschka SD, Murry CE, *et al.* In vitro generation of differentiated cardiac myofibers on micropatterned laminin surfaces. *J Biomed Mater Res.* 2002 Jun 5;60(3):472–479.
121. Thomas SP, Bircher-Lehmann L, Thomas SA, Zhuang J, Saffitz JE, Kléber AG. Synthetic strands of neonatal mouse cardiac myocytes: structural and electrophysiological properties. *Circ Res.* 2000 Sep 15;87(6):467–473.

122. Biendarra-Tiegs SM, Yechikov S, Shergill B, Brumback B, Takahashi K, Shirure VS, *et al.* An iPS-derived in vitro model of human atrial conduction. *Physiol Rep.* 2022 Sep;10(18):e15407.
123. Laksman Z, Wauchop M, Lin E, Protze S, Lee J, Yang W, *et al.* Modeling Atrial Fibrillation using Human Embryonic Stem Cell-Derived Atrial Tissue. *Sci Rep.* 2017 Jul 13;7(1):5268.
124. Nishimura S, Yasuda S, Katoh M, Yamada KP, Yamashita H, Saeki Y, *et al.* Single cell mechanics of rat cardiomyocytes under isometric, unloaded, and physiologically loaded conditions. *Am J Physiol Heart Circ Physiol.* 2004 Jul;287(1):H196–202.
125. Häneke T, Sahara M. Progress in bioengineering strategies for heart regenerative medicine. *Int J Mol Sci.* 2022 Mar 23;23(7).
126. Mishra B, Upadhyay M, Adena SR. Hydrogels: an introduction to a controlled drug delivery device, synthesis and application in drug delivery and tissue engineering. *Austin J Biomed Eng.* 2017; 4(1):1037.
127. Eschenhagen T, Fink C, Remmers U, Scholz H, Wattchow J, Weil J, *et al.* Three-dimensional reconstitution of embryonic cardiomyocytes in a collagen matrix: a new heart muscle model system. *FASEB J.* 1997 Jul;11(8):683–694.
128. Hansen A, Eder A, Bönstrup M, Flato M, Mewe M, Schaaf S, *et al.* Development of a drug screening platform based on engineered heart tissue. *Circ Res.* 2010 Jul 9;107(1):35–44.
129. Zimmermann WH, Schneiderbanger K, Schubert P, Didié M, Münzel F, Heubach JF, *et al.* Tissue engineering of a differentiated cardiac muscle construct. *Circ Res.* 2002 Feb 8;90(2):223–230.
130. Fink C, Ergün S, Kralisch D, Remmers U, Weil J, Eschenhagen T. Chronic stretch of engineered heart tissue induces hypertrophy and functional improvement. *FASEB J.* 2000 Apr;14(5):669–679.
131. Mannhardt I, Breckwoldt K, Letuffe-Brenière D, Schaaf S, Schulz H, Neuber C, *et al.* Human engineered heart tissue: analysis of contractile force. *Stem Cell Rep.* 2016 Jul 12;7(1):29–42.
132. Hirt MN, Boeddinghaus J, Mitchell A, Schaaf S, Börnchen C, Müller C, *et al.* Functional improvement and maturation of rat and human engineered heart tissue by chronic electrical stimulation. *J Mol Cell Cardiol.* 2014 Sep;74:151–161.

133. Liao B, Jackman CP, Li Y, Bursac N. Developmental stage-dependent effects of cardiac fibroblasts on function of stem cell-derived engineered cardiac tissues. *Sci Rep*. 2017 Feb 9;7:42290.
134. Tiburcy M, Hudson JE, Balfanz P, Schlick S, Meyer T, Chang Liao M-L, *et al*. Defined engineered human myocardium with advanced maturation for applications in heart failure modeling and repair. *Circulation*. 2017 May 9;135(19):1832–1847.
135. Goldfracht I, Protze S, Shiti A, Setter N, Gruber A, Shaheen N, *et al*. Generating ring-shaped engineered heart tissues from ventricular and atrial human pluripotent stem cell-derived cardiomyocytes. *Nat Commun*. 2020 Jan 7;11(1):75.
136. Eder A, Vollert I, Hansen A, Eschenhagen T. Human engineered heart tissue as a model system for drug testing. *Adv Drug Deliv Rev*. 2016 Jan 15;96:214–224.
137. Maruyama H, Yokota Y, Hosono K, Arai F. Hydrogel Heart Model with Temperature Memory Properties for Surgical Simulation. *Sensors (Basel)*. 2019 Mar 4;19(5).
138. Yokota Y, Maruyama H, Arai F. Hydrogel Heart Model Having Temperature Indicating Function. 2018 International Symposium on Micro-NanoMechatronics and Human Science (MHS) IEEE 2018; (pp. 1-2).
139. Arena CB, Szot CS, Garcia PA, Rylander MN, Davalos RV. A three-dimensional in vitro tumor platform for modeling therapeutic irreversible electroporation. *Biophys J*. 2012 Nov 7;103(9):2033–2042.
140. Wasson EM, Alinezhadbalalami N, Brock RM, Allen IC, Verbridge SS, Davalos RV. Understanding the role of calcium-mediated cell death in high-frequency irreversible electroporation. *Bioelectrochemistry*. 2020 Feb;131:107369.
141. Sato T, Stange DE, Ferrante M, Vries RGJ, Van Es JH, Van den Brink S, *et al*. Long-term expansion of epithelial organoids from human colon, adenoma, adenocarcinoma, and Barrett’s epithelium. *Gastroenterology*. 2011 Nov;141(5):1762–1772.
142. Huch M, Gehart H, van Boxtel R, Hamer K, Blokzijl F, Versteegen MMA, *et al*. Long-term culture of genome-stable bipotent stem cells from adult human liver. *Cell*. 2015 Jan 15;160(1-2):299–312.

143. Gao D, Vela I, Sboner A, Iaquina PJ, Karthaus WR, Gopalan A, *et al.* Organoid cultures derived from patients with advanced prostate cancer. *Cell*. 2014 Sep 25;159(1):176–187.
144. Murphy WL, McDevitt TC, Engler AJ. Materials as stem cell regulators. *Nat Mater*. 2014 Jun;13(6):547–557.
145. Kumar A, Starly B. Large scale industrialized cell expansion: producing the critical raw material for biofabrication processes. *Biofabrication*. 2015 Nov 5;7(4):044103.
146. Tung Y-C, Hsiao AY, Allen SG, Torisawa Y, Ho M, Takayama S. High-throughput 3D spheroid culture and drug testing using a 384 hanging drop array. *Analyst*. 2011 Feb 7;136(3):473–478.
147. Hoarau-Véchet J, Rafii A, Touboul C, Pasquier J. Halfway between 2D and Animal Models: Are 3D Cultures the Ideal Tool to Study Cancer-Microenvironment Interactions? *Int J Mol Sci*. 2018 Jan 18;19(1).
148. Yuhas JM, Li AP, Martinez AO, Ladman AJ. A simplified method for production and growth of multicellular tumor spheroids. *Cancer Res*. 1977 Oct;37(10):3639–3643.
149. Tseng H, Gage JA, Raphael RM, Moore RH, Killian TC, Grande-Allen KJ, *et al.* Assembly of a three-dimensional multitype bronchiole coculture model using magnetic levitation. *Tissue Eng Part C Methods*. 2013 Sep;19(9):665–675.
150. Rawal P, Tripathi DM, Ramakrishna S, Kaur S. Prospects for 3D bioprinting of organoids. *Bio-des Manuf*. 2021 Jan 28; 4, 627-640.
151. Cui H, Nowicki M, Fisher JP, Zhang LG. 3D bioprinting for organ regeneration. *Adv Healthc Mater*. 2017 Jan;6(1).
152. Pollen AA, Bhaduri A, Andrews MG, Nowakowski TJ, Meyerson OS, Mostajir-Radji MA, *et al.* Establishing Cerebral Organoids as Models of Human-Specific Brain Evolution. *Cell*. 2019 Feb 7;176(4):743–756.e17.
153. Huch M, Knoblich JA, Lutolf MP, Martinez-Arias A. The hope and the hype of organoid research. *Development*. 2017 Mar 15;144(6):938–941.
154. de Souza N. Organoids. *Nat Methods*. 2018 Jan 3;15(1):23–23.
155. Munsie M, Hyun I, Sugarman J. Ethical issues in human organoid and gastruloid research. *Development*. 2017 Mar 15;144(6):942–945.

156. Whitesides GM. The origins and the future of microfluidics. *Nature*. 2006 Jul 27;442(7101):368–373.
157. Wang L, Liu W, Wang Y, Wang J, Tu Q, Liu R, *et al*. Construction of oxygen and chemical concentration gradients in a single microfluidic device for studying tumor cell-drug interactions in a dynamic hypoxia microenvironment. *Lab Chip*. 2013 Feb 21;13(4):695–705.
158. Ho C-T, Lin R-Z, Chen R-J, Chin C-K, Gong S-E, Chang H-Y, *et al*. Liver-cell patterning lab chip: mimicking the morphology of liver lobule tissue. *Lab Chip*. 2013 Sep 21;13(18):3578–3587.
159. Sung JH, Shuler ML. A micro cell culture analog (μ CCA) with 3-D hydrogel culture of multiple cell lines to assess metabolism-dependent cytotoxicity of anti-cancer drugs. *Lab Chip*. 2009;9(10):1385.
160. Sung JH, Wang YI, Narasimhan Sriram N, Jackson M, Long C, Hickman JJ, *et al*. Recent Advances in Body-on-a-Chip Systems. *Anal Chem*. 2019 Jan 2;91(1):330–351.
161. Zhao Y, Rafatian N, Wang EY, Feric NT, Lai BFL, Knee-Walden EJ, *et al*. Engineering microenvironment for human cardiac tissue assembly in heart-on-a-chip platform. *Matrix Biol*. 2020;85-86:189–204.
162. Chugh SS, Havmoeller R, Narayanan K, Singh D, Rienstra M, Benjamin EJ, *et al*. Worldwide epidemiology of atrial fibrillation: a Global Burden of Disease 2010 Study. *Circulation*. 2014 Feb 25;129(8):837–847.
163. January CT, Wann LS, Calkins H, Chen LY, Cigarroa JE, Cleveland JC, *et al*. 2019 AHA/ACC/HRS focused update of the 2014 AHA/ACC/HRS guideline for the management of patients with atrial fibrillation: A report of the american college of cardiology/american heart association task force on clinical practice guidelines and the heart rhythm society. *J Am Coll Cardiol*. 2019 Jul 9;74(1):104–132.
164. Morillo CA, Banerjee A, Perel P, Wood D, Jouven X. Atrial fibrillation: the current epidemic. *J Geriatr Cardiol*. 2017 Mar;14(3):195–203.
165. Avazzadeh S, McBride S, O'Brien B, Coffey K, Elahi A, O'Halloran M, *et al*. Ganglionated plexi ablation for the treatment of atrial fibrillation. *J Clin Med*. 2020 Sep 24;9(10).

166. Grimaldi M, Di Monaco A, Gomez T, Berman D, Datta K, Sharma T, *et al.* Time Course of Irreversible Electroporation Lesion Development Through Short- and Long-Term Follow-Up in Pulsed-Field Ablation-Treated Hearts. *Circ Arrhythm Electrophysiol.* 2022 Jul;15(7):e010661.
167. Maan A, Koruth J. Pulsed field ablation: a new paradigm for catheter ablation of arrhythmias. *Curr Cardiol Rep.* 2022 Feb;24(2):103–108.
168. Yamane T. Catheter ablation of atrial fibrillation: Current status and near future. *J Cardiol.* 2022 Feb 24;
169. van Es R, Konings MK, Du Pré BC, Neven K, van Wessel H, van Driel VJHM, *et al.* High-frequency irreversible electroporation for cardiac ablation using an asymmetrical waveform. *Biomed Eng Online.* 2019 Jun 20;18(1):75.
170. Wittkamp FHM, van Es R, Neven K. Electroporation and its relevance for cardiac catheter ablation. *JACC Clin Electrophysiol.* 2018 Aug;4(8):977–986.
171. Lavee J, Onik G, Mikus P, Rubinsky B. A novel nonthermal energy source for surgical epicardial atrial ablation: irreversible electroporation. *Heart Surg Forum.* 2007;10(2):E162–7.
172. Reddy VY, Neuzil P, Koruth JS, Petru J, Funosako M, Cochet H, *et al.* Pulsed field ablation for pulmonary vein isolation in atrial fibrillation. *J Am Coll Cardiol.* 2019 Jul 23;74(3):315–326.
173. Tan NY, Ladas TP, Christopoulos G, Sugrue AM. Ventricular nanosecond pulsed electric field delivery using active fixation leads: a proof-of-concept preclinical study. *Journal of Interventional Cardiac Electrophysiology*, 2022; 1-11.
174. Varghese F, Philpott JM, Neuber JU. Surgical Ablation of Cardiac Tissue with Nanosecond Pulsed Electric Fields in Swine. *Cardiovascular* 2022;
175. Avazzadeh S, O’Brien B, Coffey K, O’Halloran M, Keane D, Quinlan LR. Establishing irreversible electroporation electric field potential threshold in A suspension in vitro model for cardiac and neuronal cells. *J Clin Med.* 2021 Nov 22;10(22).
176. Hunter DW, Kostecki G, Fish JM, Jensen JA, Tandri H. In vitro cell selectivity of reversible and irreversible: electroporation in cardiac tissue. *Circ Arrhythm Electrophysiol.* 2021 Apr;14(4):e008817.

177. Vu TD, Kofidis T. Biomaterials and cells for cardiac tissue engineering. *Cardiac regeneration and repair*. 2014;
178. Prieto JL, Su H-W, Hou HW, Vera MP, Levy BD, Baron RM, *et al.* Monitoring sepsis using electrical cell profiling. *Lab Chip*. 2016 Nov 1;16(22):4333–4340.
179. McBride S, Avazzadeh S, Wheatley AM, O'Brien B, Coffey K, Elahi A, *et al.* Ablation Modalities for Therapeutic Intervention in Arrhythmia-Related Cardiovascular Disease: Focus on Electroporation. *J Clin Med*. 2021 Jun 16;10(12).
180. Weaver JC. Electroporation of cells and tissues. *IEEE Trans Plasma Sci*. 2000;28(1):24–33.
181. Kaminska I, Kotulska M, Stecka A, Saczko J, Drag-Zalesinska M, Wysocka T, *et al.* Electroporation-induced changes in normal immature rat myoblasts (H9C2). *Gen Physiol Biophys*. 2012 Mar;31(1):19–25.
182. Sugrue A, Maor E, Ivorra A, Vaidya V, Witt C, Kapa S, *et al.* Irreversible electroporation for the treatment of cardiac arrhythmias. *Expert Rev Cardiovasc Ther*. 2018 May;16(5):349–360.
183. Mercadal B, Beitel-White N, Aycock KN, Castellví Q, Davalos RV, Ivorra A. Dynamics of Cell Death After Conventional IRE and H-FIRE Treatments. *Ann Biomed Eng*. 2020 May;48(5):1451–1462.
184. Xie F, Varghese F, Pakhomov AG, Semenov I, Xiao S, Philpott J, *et al.* Ablation of myocardial tissue with nanosecond pulsed electric fields. *PLoS One*. 2015 Dec 14;10(12):e0144833.
185. Qin Q, Xiong Z-A, Liu Y, Yao C-G, Zhou W, Hua Y-Y, *et al.* Effects of irreversible electroporation on cervical cancer cell lines in vitro. *Mol Med Rep*. 2016 Sep;14(3):2187–2193.
186. Vogel JA, van Veldhuisen E, Agnass P, Crezee J, Dijk F, Verheij J, *et al.* Correction: Time-Dependent Impact of Irreversible Electroporation on Pancreas, Liver, Blood Vessels and Nerves: A Systematic Review of Experimental Studies. *PLoS One*. 2017 Mar 10;12(3):e0174018.
187. Beebe SJ. Regulated and apoptotic cell death after nanosecond electroporation. *Handbook of electroporation Heidelberg: Springer International Publishing*, 2017; 511-28.

188. Yatim N, Cullen S, Albert ML. Dying cells actively regulate adaptive immune responses. *Nat Rev Immunol*. 2017 Apr;17(4):262–275.
189. Kapałczyńska M, Kolenda T, Przybyła W. 2D and 3D cell cultures—a comparison of different types of cancer cell cultures. *Arch Med Sci* 14: 910–919. 2016;
190. Varaprasad K, Raghavendra GM, Jayaramudu T, Yallapu MM, Sadiku R. A mini review on hydrogels classification and recent developments in miscellaneous applications. *Mater Sci Eng C Mater Biol Appl*. 2017 Oct 1;79:958–971.
191. Baker BM, Chen CS. Deconstructing the third dimension: how 3D culture microenvironments alter cellular cues. *J Cell Sci*. 2012 Jul 1;125(Pt 13):3015–3024.
192. Pucihar G, Kotnik T, Kanduser M, Miklavcic D. The influence of medium conductivity on electroporation and survival of cells in vitro. *Bioelectrochemistry*. 2001 Nov;54(2):107–115.
193. Rodell CB, MacArthur JW, Dorsey SM, Wade RJ, Wang LL, Woo YJ, *et al*. Shear-Thinning Supramolecular Hydrogels with Secondary Autonomous Covalent Crosslinking to Modulate Viscoelastic Properties In Vivo. *Adv Funct Mater*. 2015 Jan 28;25(4):636–644.
194. Schanté CE, Zuber G, Herlin C, Vandamme TF. Chemical modifications of hyaluronic acid for the synthesis of derivatives for a broad range of biomedical applications. *Carbohydr Polym*. 2011 Jun;85(3):469–489.
195. Ramachandran GN. Molecular structure of collagen. *Int Rev Connect Tissue Res*. 1963;1:127–182.
196. Naahidi S, Jafari M, Logan M, Wang Y, Yuan Y, Bae H, *et al*. Biocompatibility of hydrogel-based scaffolds for tissue engineering applications. *Biotechnol Adv*. 2017 Sep;35(5):530–544.
197. Kleinman HK, Klebe RJ, Martin GR. Role of collagenous matrices in the adhesion and growth of cells. *J Cell Biol*. 1981 Mar;88(3):473–485.
198. Neal RE, Millar JL, Kavnoudias H, Royce P, Rosenfeldt F, Pham A, *et al*. In vivo characterization and numerical simulation of prostate properties for non-thermal irreversible electroporation ablation. *Prostate*. 2014 May;74(5):458–468.

199. Weaver JC, Smith KC, Esser AT, Son RS, Gowrishankar TR. A brief overview of electroporation pulse strength-duration space: a region where additional intracellular effects are expected. *Bioelectrochemistry*. 2012 Oct;87:236–243.
200. Peyman A, Gabriel C, Grant EH. Complex permittivity of sodium chloride solutions at microwave frequencies. *Bioelectromagnetics: Journal of the Bioelectromagnetics Society, The Society for Physical Regulation in Biology and Medicine, The European Bioelectromagnetics Association*, 2007; 28(4), 264-274.
201. Ištuk N, Gioia AL, Benchakroun H. Relationship Between the Conductivity of Human Blood and Blood Counts. *IEEE Journal of Electromagnetics, RF and Microwaves in Medicine and Biology*, 2021; 6(2):184-190.
202. Petrella RA, Fesmire CC, Kaufman JD, Topasna N, Sano MB. Algorithmically controlled electroporation: A technique for closed loop temperature regulated pulsed electric field cancer ablation. *IEEE Trans Biomed Eng*. 2020 Aug;67(8):2176–2186.
203. Ivey JW, Latouche EL, Sano MB, Rossmeis JH, Davalos RV, Verbridge SS. Targeted cellular ablation based on the morphology of malignant cells. *Sci Rep*. 2015 Nov 24;5:17157.
204. Sieni E, Bazzolo B, Pieretti F, Zamuner A, Tasso A, Dettin M, *et al*. Breast cancer cells grown on hyaluronic acid-based scaffolds as 3D in vitro model for electroporation. *Bioelectrochemistry*. 2020 Dec;136:107626.